# MCCE CALCULATION OF QUINONE DEPENDENT ELECTRON AND PROTON TRANSFERS IN *Rhodobacter sphaeroides* BACTERIAL PHOTOSYNTHETIC REACTION CENTERS

by

**ZHENYU ZHU**

A dissertation submitted to the Graduate Faculty in Physics in partial fulfillment of the requirements for the degree of Doctor of Philosophy, The City University of New York

2005

This manuscript has been read and accepted for the Graduate Faculty in Physics in satisfaction of the dissertation requirements for the degree of Doctor of Philosophy.

12/20/04
Date

Chair of Examining Committee

1/11/05
Date

Executive Officer

**R. Callender**

**T. Boyer**

**H. Makes**

Supervisory Committee

THE CITY UNIVERSITY OF NEW YORK

# ABSTRACT

MCCE CALCULATION OF QUINONE DEPENDENT ELECTRON AND PROTON TRANSFERS IN *Rhodobacter sphaeroides* BACTERIAL PHOTOSYNTHETIC REACTION CENTERS

by

ZHENYU ZHU

Adviser: Professor Marilyn Gunner

To investigate the proton coupled electron transfers in membrane proteins such as photosynthetic reaction centers (RCs), Multiple Conformational Continuum Electrostatics (MCCE) was used to calculate the redox midpoint potentials and $pK_a$ of ubiquinone at $Q_A$ and $Q_B$ binding sites in the structures of *Rhodobacter sphaeroides* RCs.

By using 1AIJ(G) X-ray crystal structure, the calculated $Q_A$ $E_m$ is –40 mV, the proximal $Q_B$ $E_m$ is –10 mV, and the distal $Q_B$ $E_m$ is –260 mV. In addition, the electrochemistry of the second reduction in the $Q_B$ site was calculated. The reaction $Q_A^-Q_B^- \rightarrow Q_AQ_B^{-2}$ is about 200 meV less favorable than $Q_A^-Q_B^- \rightarrow Q_A^-Q_BH$, supporting the Proton Transfer and Electron Transfer (PTET) mechanism where protonation of $Q_B^-$ precedes electron transfer. The calculations also confirm that the first protonation of $Q_B$ occurs at the distal $Q_B$ oxygen and the second binds to the proximal oxygen. SerL223 electrostatically stabilizes the semiquinone $Q_BH$ and destabilizes $Q_BH_2$.

By MCCE calculations on multiple X-ray crystal structures (1AIJ(G), 1M3X, 1PCR′), the average $Q_A$ $E_m$ is –35±7 mV, and the average proximal $Q_B$ $E_m$ is 24±27 mV.

The $E_m$s are relatively independent of and are in good agreement with the experimental data. However, MCCE simulations show significant differences in the ionization states of $Q_B$ pocket residues AspL210, GluL212, AspL213 and GluH173 in the ground state due to small changes in the different crystal structures. When $Q_B$ is reduced the ionization states are identical in all structures. Thus, the intra-cluster proton transfers required for electron transfer vary with small changes in structure.

# ACKNOWLEDGMENTS

I owe special gratitude to my thesis advisor Dr. Marilyn Gunner for her four-year of academic education, guidance, encouragement and support; for giving me such a great opportunity to work in the field of computational biophysics.

I am very grateful to the Physics Department of City College of New York and NSF. Without their financial support, I could not finish my PH.D degree.

I would like to thank all other members of my examine committee, Professors Hernan Makes, Timothy Boyer and Robert Callender for their valuable time and suggestions.

I also very much thank to all our group members. Their help and support are so valuable to my calculations. We had a great experience working together. I will not forget the hot arguments and long discussions in the group meetings and workshops.

Finally, I would like to thank my wife and parents, for their great support and patience over years.

# TABLE OF CONTENTS

# ABBREVIATIONS

All free energy terms $\Delta G$ and electrochemical midpoints ($E_m$) refer to standard conditions at pH 7 ($\Delta G^{\circ\prime}$ and $E^{\circ\prime}_{m,7}$). 1.36 kcal/mole = 59.3 meV is the energy to change a $pK_a$ by 1 pH unit at 20°C. $pK_a'$ the $pK_a$ calculated from the free energy of protonation at pH 7.

# LIST OF TABLES

# LIST OF FIGURES

# Chapter 1 Introduction

## 1.1 Bacterial Reaction Centers

### 1.1.1 Importance of RC structures

The bacterial reaction center (RC) was the first transmembrane protein to be known to atomic resolution, with a 3Å resolution structure (*1*) that circulated among excited scientists in 1985 and was deposited in the data bank as PDB code 1PRC. Michel, Deisenhofer, and Huber won the Nobel Prize for this work in 1988. Currently there are around 40 structures of bacterial reaction centers as well as structures of the green plant PSI and PSII for comparison. The importance of those molecules stem from the fact that they provide the energy on which almost all life on earth depends, namely they allow plants and some (so-called photosynthetic) bacteria to harness the sun's electromagnetic energy and convert it into chemical energy that all biological organisms can use. The bacterial reaction center is undoubtedly one of the most heavily studied electron transfer proteins. RCs research has given rise to unique contributions to our understanding of biological electron transfer and coupled protonation reactions, and has provided fascinating information about the basic properties of natural photosynthesis such as the dynamic roles played by the protein to catalyze the conversion of solar energy into a form that can be used by the cell.

Reaction Centers are complexes of pigment proteins that vary greatly in their composition and complexity. They can be found in plants, algae and a variety of bacteria species. Based on their subunit compositions, bacterial RC complexes are classified into two groups: RCs of Group I are composed of only three major subunits (L, M and H)

(e.g. *Rhodobacter sphaeroides*), and RCs of Group II possess an additional peripheral cytochrome subunit (e.g. *Rhodopseudomonas virids*). Several independent structures for RC of this bacterium have been solved. Because the protocols for genetic engineering in *Rhodobacter sphaeroides* were developed much earlier than in other bacteria, much of our knowledge of the role of individual residues has come from the study of modified function in mutant strains engineered with specific residue changes. The bacterial RC structures of *Rhodobacter sphaeroides* have been solved with several different substrate reactants, so that the changes in structure associated with turn-over of the catalytic site have been revealed. Our bacterial RC calculations are based on this species. The native PDB (Protein Data Bank, which provides the coordinates of all atoms) files of *Rhodobacter sphaeroides* are 2RCR, 4RCR, 1PSS, 1PCR and 1YST, while the mutated structures of this species are 1PST, 1MPS, 1OOV, 1E14 and 1E6D, *etc*. In 1997, two light-induced structures 1AIJ and 1AIG were solved at 2.2 and 2.6Å resolution respectively (*2*), a movement of secondary quinone $Q_B$ from an inactive distal position (distal site $Q_{BD}$) (1AIJ) to an active proximal binding site (proximal site $Q_B$) (1AIG) was seen to be the major structure difference between them. In 2002, another structure of bacterial RC from *Rhodobacter Sphaeroides* was available at 2.55 Å resolution as 1M3X (*3*), it included three extra lipid molecules that lie on the surface of the protein, two of them are in close contact with the cofactors. Recently, 1PCR′ (*4*) was resolved with higher resolution of 1.87 Å. These high-resolution structures provide an opportunity to understand on an atomic level how the protein controls the free energy of electron and proton transfer reactions.

**Figure 1.1.** The crystal structure and cofactors of bacterial RCs.

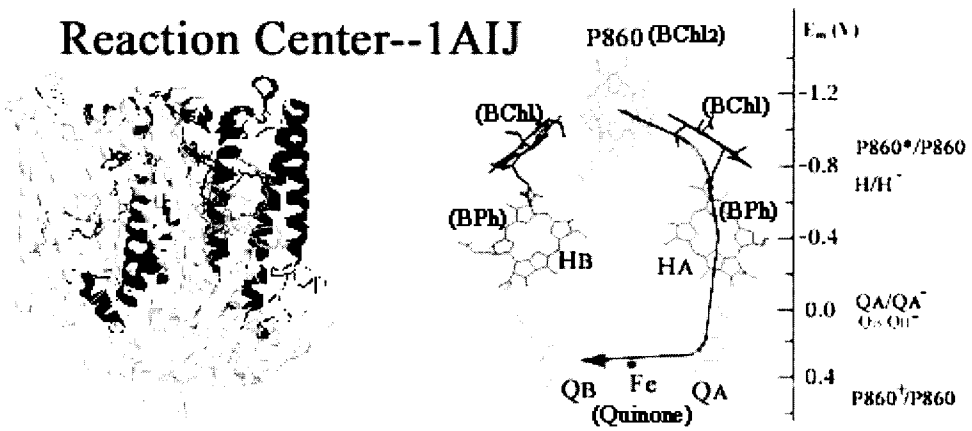


From bacterial RC structure *Rb. sphaeroides* 1AIJ.

### 1.1.2. Structure and Function of Bacterial RC

The structure of the bacterial reaction center is shown in Fig 1.1, oriented with the cytoplasmic domain at bottom. The complex is made up of three protein subunits (L, M and H) and 10 cofactors. Each L and M subunit has five transmembrane α-helices, while the H subunit has one transmembrane α-helix.

The arrangement of cofactors in the bacteria RCs is also shown in Fig 1.1. On one side of the RC near the periplasmic surface is the bacteriochlorophylls dimer that serves as the primary electron donor (P). Two sets of cofactors involving bacteriochlorophyll (BChl), bacteriopheophytins (BPh) and ubiquione (Q) are arranged in two branches (labeled as A and B) spanning the membrane. The primary electron transfer occurs predominantly along the A branch from the bacteriochlorophyll dimer, Bchl2 through BChl, BPh, the primary quinone $Q_A$, to the secondary quinone $Q_B$, The electron transfer from $Q_A$ to $Q_B$ spans a distance 15 Å (edge to edge). The two quinone molecules are linked by H-bonds through a His-$Fe^{2+}$-His complex.

In *Rb. sphaeroides* RC, the process is initiated by a light-induced excitation of a bacteriochlorophyll dimer (P). An exited electron is then transferred sequentially from P to a bacteria pheophytin (BPh, $H_A$), to a primary ubiquinone acceptor ($Q_A$) and a secondary ubiquinone acceptor ($Q_B$). At each transfer step the electron is stabilized against change recombination for progressively long times. The full reduction of the quinone ($Q_B$) to dihydroquinone ($Q_BH_2$) requires the transfer of two electrons and is coupled to uptake of two protons from the cytoplasmic side to the proton gradient.

$$Q_B + 2e^- + 2H^+ \Rightarrow Q_BH_2 \qquad (1.1)$$

Following reduction, the dihydroquinone is released from the RC into the membrane and reoxidized by the cytochrome *bc*1 complex, releasing protons on the opposite side of the membrane. The transport of protons across the membrane is coupled to cycling of the electron back to the Reaction Center via a cytochrome *c* molecule. The two proteins together function as light induced proton pump which gives rise to a transmembrane proton gradient that is utilized for ATP synthesis.

### 1.1.3 Proton-coupled Electrons Transfer in Bacterial RCs

The bound ubiquinone ($Q_{10}$) molecule, called $Q_B$, displays the most complex redox chemistry of all of the RC cofactors, undergoing a double reduction that coupled with binding two protons from the crytoplasmic side of membrane (*5*). The quinone can exist in three main redox states: unreduced quinone (Q), partially reduced semiquinone ($Q^-$) and fully reduced and protonated dihydroquinone ($QH_2$). Totally, quinone chemistry allowes nine possible states for the quinone at the $Q_B$ binding sites during the reduction and protonation of Q to $QH_2$ as shown in Fig. 1.2.

**Figure 1.2.** Nine quinone states during the reduction and protonation of Q to $QH_2$.

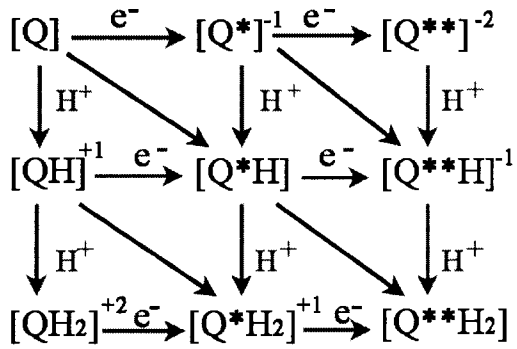

Although $Q_A$ and $Q_B$ in bacterial RC of *Rb. sphaeroides* are identical ubiquinone-10 molecules, $Q_A$ can only be reduced to semiquinone and never become protonated, $Q_B$ accepts two electrons and takes up two protons from on two turnovers of RC. Their difference *in situ* thermodynamic properties of the two quinones can be attributed to different protein environment. $Q_B$ is surround by a cluster of polar residues, acids and waters, including SerL223, AspL210, GluL212, AspL213, GluH173, AsnM44 and AspM17. Those residues have been identified as important for electron and proton transfer by both mutation experiments (*6-12*) and simulations (*13, 14*).

**Figure 1.3.** The binding site of $Q_A$ and proximal $Q_B$ in bacterial RCs.

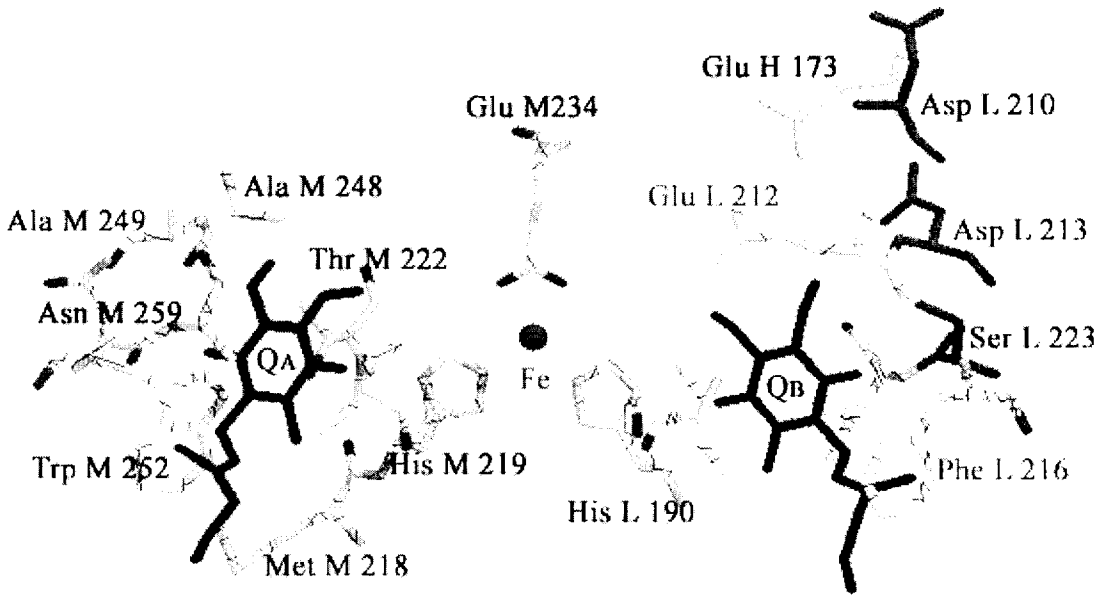

**Figure 1.4.** The quinone reduction cycle in bacterial RCs (*5*)

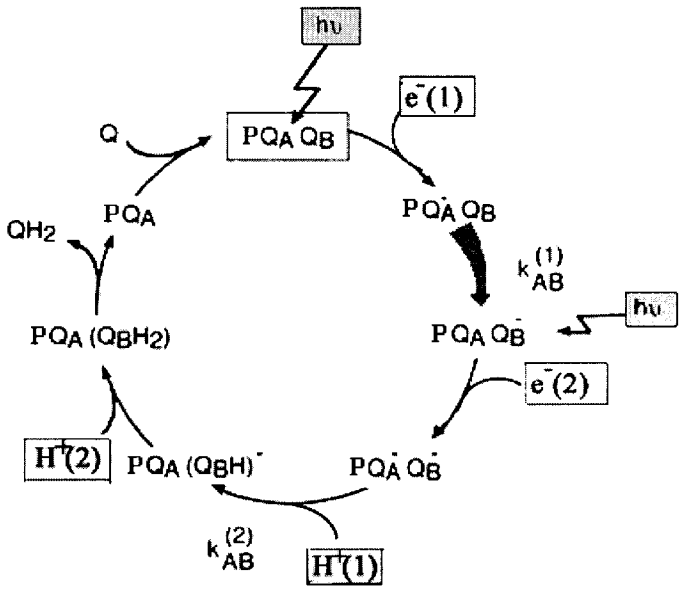


Each step in the cycle represents a change in the state of $Q_A$ or $Q_B$ due to electron transfer or proton binding. The initial state $PQ_AQ_B$ is shown at the top of the cycle. The first step is the photochemical reduction of $Q_A$, forming the state $PQ_A^-Q_B$, followed by reduction of $P^+$ by transferring an electron from cytochrome *c*. The second step is the electron transfer from $Q_A^-$ to $Q_B$ with the rate $k_{AB}^{(1)}$, forming the photochemically active $PQ_AQ_B^-$. In this step, the electron transfer rate is measurable and our first electron transfer simulation will focus on this reaction. The third step represents the photoinduced second electron transfer resulting in reduction of $Q_A$ to form $PQ_A^-Q_B^-$. The forth step is the proton-coupled second electron transfer reaction $k_{AB}^{(2)}$. The overall reaction results in the transfer of the semiquinone $Q_B^-$ to form $PQ_AQ_BH^-$. This occurs in two sequential reactions: protonation of the semiquinone $Q_B^-$ to form the protonated intermediate semiquinone, $Q_BH$, followed by electron transfer or electron transfer first to form dihydroquinone $Q_B^{-2}$ followed by protonation. The next step is the binding of the second proton, giving rise to the dihydroquinone. After the formation of $QH_2$ at the $Q_B$ site, the $QH_2$ dissociate into the membrane with the rebinding of a quinone to reform the initial state.

## 1.2 The Current State of Calculations on Bacterial RCs

Residue side-chain $pK_a$ and quinone midpoint potential $E_m$ simulations of bacterial RC have been attempted by a number of methods to better understand the functional properties of protein at the atomic level. There are several current computational methods used to explore the protein from structure to function in atomic level. Chemical Quantum Mechanics (QM/MM) can model the basic chemical reaction and decide the electron density distribution in micro-systems. Currently it can only focus on cofactor and local clusters of residues around the cofactors (*15-18*). Molecule Dynamics (MD), has been used to study $Q_B$ movements (*19*), conformational gating (*20*) and changes in protonation states of amino acids GluL212 and AspL213 on the first electron transfer (*21*). Continuum Electrostatics (CE) provides rapid estimates of long-range electrostatic interactions by averaging many motions into the electrostatic dielectric constant (*22, 23*). The first electron transfer from $Q_A^-$ to $Q_B$ has been studied by various CE methods using both *Rps. viridis* (*24, 25*) and *Rb. sphaeroides* RC structures (*13, 14, 26-28*). The energetics of the second $Q_B$ electron transfers have also been calculated by Knapp and coworkers with a CE model in *Rps. viridis* (*25*) and *Rb. sphaeroides* (*27*) RCs.

Standard continuum electrostatics techniques provide two types of response to the changing of charges such as with quinone reduction (*22, 23, 29*). One is a homogeneous dielectric response defined by the dielectric constant used in the calculation. Values from 4 to 20 have been used with the higher values averaging more changes in the protein. The other is the changes in protonation of surrounding residues which are analyzed using standard methods to residue calculate $pK_a$s (*29-31*). However, no explicit conformational

changes are allowed. Multiple Conformation Continuum Electrostatics (MCCE) adds side-chain heavy atom and hydroxyl conformers to improve the flexibility of the CE model (*32-35*). This method can follow linked conformational and ionization state changes during the reduction of quinone.

# Chapter 2 Methods and materials

## 2.1 Continuum Electrostatic Model

Classical electrostatics takes its simplest form when it considers only charges in vacuum. Such a system is described by Poisson's equation in the following form:

$$-\nabla \cdot \nabla\phi(\vec{r}) = \frac{\rho(\vec{r})}{\varepsilon_o} \tag{2.1}$$

$$\vec{E}(\vec{r}) = -\nabla\phi(\vec{r}) \tag{2.2}$$

Here $\phi(\vec{r})$ and $\rho(\vec{r})$ are, respectively, the electrostatic potential and the charge density as a function of position, and r is the coordinates of a point in space. For a point-charge, $\rho(\vec{r})$ has the form of a δ-function. $\varepsilon_o$ is the permitivity of free space. Intuitively, this equation says that charges are the source of the electrical field, since $-\nabla \cdot \nabla\phi(\vec{r})$ represents the divergence of the E field. Solutions of eqn. 2.1 yield the familiar Coulomb's law. The useful superposition principle can be deduced from eqn. 2.1. This states that the total electrostatic field produced by a system of charges is the arithmetic sum of the fields produced by the individual charges. Thus, the field is the superposition of the individual fields.

The electrostatic interactions among charges in a uniform medium (gas, liquid, or solid) are usually weakened relative to those for the same charges in vacuum. Often to a good approximation, the field is reduced everywhere by a constant factor known as the dielectric constant D. For a charge in a medium of uniform dielectric constant, the following form of the Poisson equation is appropriate:

$$-\nabla \cdot \nabla\phi(\vec{r}) = \frac{\rho(\vec{r})}{\varepsilon_o D} \tag{2.3}$$

It is apparent that the potentials that result from the eqn. 2.1 are just 1/D of their values in vacuum for the same charge distribution $\rho(\vec{r})$, the energies are reduced by the same factor.

An atom or molecule in an externally imposed electric field develops a nonzero net dipole moment or if the molecule already has a nonzero dipole moment, the external electric field increases it further. The magnitude of a dipole moment is a measure of charge separation. (Thus, an electron and proton separated by 1 Å possess a dipole moment of 1 electron- Angstrom (or, in SI units, $1.65 \times 10^{-29}$ Coulomb-meters.) Thus, the atoms or molecules in material develop dipole moments when the material is exposed to an electrical field. The field generated by these induced dipoles runs opposite to the inducing field. As a consequence, the overall field is weakened, as expected for a dielectric medium.

Fig. 2.1 illustrates how a dielectric medium weakens the field due to a positive charge. The dipoles induced in the material are aligned with the inducing field. The charges at the heads and tails of the induced dipoles cancel each other except at the surface of the inducing charge. This leaves a net surface charge that produces a field opposite to that of the inducing charge.

**Figure 2.1.** Positive Charge in a dielectric medium induces dipoles.

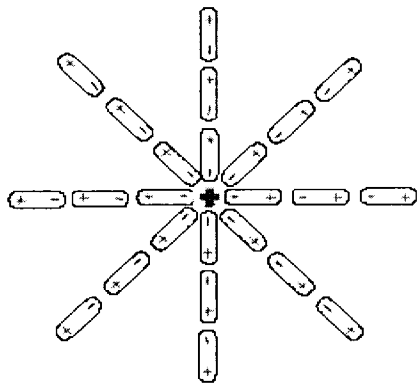

**Figure 2.2.** The Continuum Electrostatics Model and MCCE.

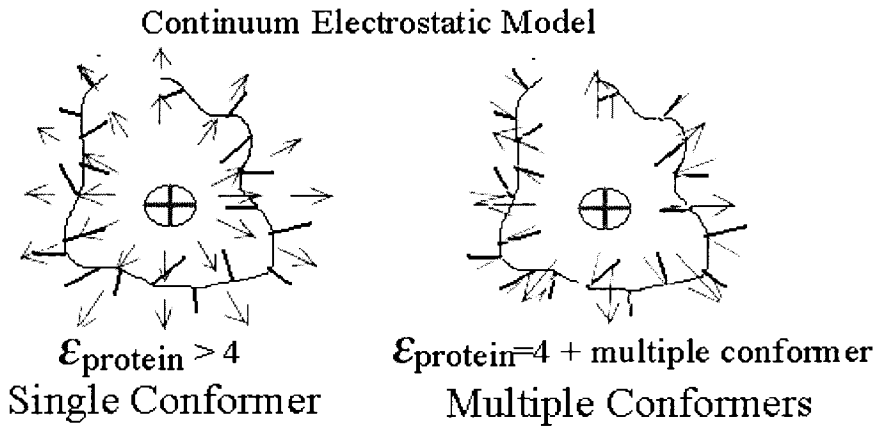


The arrows present the electrostatic force fields produced by the central charge. The lines present residue conformers.

In material, the dipole moment per unit volume is a vector field known as the polarization vector $P(\vec{r})$. In many materials, the polarization is proportional to the inducing field over a wide range of inducing fields $\vec{E}(\vec{r})$, and the constant of proportionality is the susceptibility $\chi$: $\vec{P}(\vec{r}) = \chi\vec{E}(\vec{r})$. When this proportionality holds, the dielectric response is said to be linear.

There are two chief ways that an atom or a molecule can develop a dipole moment in response to an inducing field: electronic polarization and orientational polarization. Electronic polarization occurs when the inducing field shifts the positively charged nucleus of an atom in the direction of the inducing field and the negatively charged electrons in the opposite direction, creating a dipole. Every atom can be polarized in this way. Electronic polarization rises linearly with the inducing field up to very high field strengths. In general this produces value of D near 2.

Orientational polarizability is limited to molecules that have significant permanent dipole moments; i.e., molecules that have a dipole moment even in the absence of an inducing field. Water is a good example of such a molecule. In the absence of an inducing field, a water molecule in liquid water tumbles randomly due to thermal motion. As a consequence, its time-averaged dipole moment is zero. However, in the presense of an electrical field, the tumbling of the molecular is biased in the direction of the external electric field, leading to a nonzero time-averaged dipole moment along the field. The orientational polarizability yields dielectric constant for water around 80.

Continuum Electrostatics is widely used for computing electrostatic energies of protein folding, binding and conformational changes. This model considers the protein as a rigid continuum dielectric region where partial charges are embedded. Dielectric

constant is assigned which is an approximation that averages of the polarizability of the protein medium. This includes backbone dipole distribution, side chain flexibility and atomic contribution due to thermodynamic vibration. Measurements show the dielectric constant of dried protein films and powders to range from 2.5-3.5, but those values are expected to be more variable in hydrated proteins. The electrostatic interaction of two charges is controlled by not only the dielectric constant of the material along a line joining the two charges, but also is strongly influenced by the complete distribution of dielectric media near the charges. So waters surrounding the protein effect the effective inter-protein dielectric constant.

Obviously, the assumption that protein structure is rigid and has a uniform dielectric constant is a very simple and vague approximation. While protein computations have succeeded by using different dielectric constants to simulate different region of protein, different amino acid (*34*) or by using different dielectric constants to simulate different proteins (*36*). The values used for the dielectric constant in calculations range from 30 to 2. In contrast, MCCE gives each residue several conformers and sets the background dielectric constant as a fixed low number (4 in my calculation) to account for flexibility that we do not include explicitly (see Fig. 2.2). The effective dielectric constant distribution now depends on the geometry of protein backbone and amino acids type and protein packing around each flexible residue. So MCCE can give a more precise simulation of protein flexibility than original continuum electrostatic model. MCCE can also evaluate the ionization states of all residues throughout the protein and show the dependence of residues positions and ionization states. And MCCE can give a more

precise simulation of dielectric constant distribution within the protein than other current continuum electrostatic models.

## 2.2 Multiple Conformation Continuum Electrostatic Methods (MCCE)

MCCE (*13, 23, 34, 35*) calculates the equilibrium distribution of conformation and ionization states of protein side chains, buried waters, ions, and ligands at a defined solution pH and $E_h$. Pre-selected choices for atomic coordinates and ionization states are used. Side-chain conformers are added providing alternative positions of hydroxyl protons of His, Ser, Tyr, Thr and water, and the different ionization states of the acids Asp, Glu, Tyr, Arg, Lys and His. There are at least two $Q_B$ binding sites (*37*), best characterized in a comparison of protein frozen in the light (1AIG) and dark (1AIJ) (*2*). The protein structure file 1AIJ with resolution of 2.2 Å used in this calculation, has the quinone in the distal position, The proximal $Q_B$ position of 1AIG was added into the 1AIJ structure by superimposing the $Q_B$ ring, non-heme iron and the backbone atoms of GluL212 and AspL213 (We call this Protein Data File as 1AIJ(G)). Conformers of protonated quinone species are generated with 2 different hydrogen positions for each carbonyl oxygen in the plane of the quinone ring with an angle 60° between them (Fig. 2.5). This generates 4 neutral semiquinone (QH) and 4 dihydroquinone ($QH_2$) conformers.

Lipid and detergent molecules are removed from the structure. The 110 waters with <10Å exposed surface area defined by SURFV (*38, 39*) are included. Conflicts between waters at nearby positions in a given site are avoided by providing each water with a conformer that does not interact with the protein. Thus, each water molecule is allowed to leave the protein during the Monte Carlo sampling. The Hartree-Fock partial charges are used for each ubiquinone redox state (*25*). A +2 charge is placed on the non-heme iron between $Q_A$ and $Q_B$. The partial charges for all other cofactors are from (*40*).

PARSE partial charges and radii (*41*) are used for all other groups. For calculations involving $Q_A$ or proximal $Q_B$ no quinone conformers are allowed in the distal $Q_B$ site ($Q_{BD}$). For analysis of $Q_{BD}$ the proximal $Q_B$ site is kept unoccupied. For states where the quinone is protonated conformers with different proton positions are allowed and their occupancy summed. Unless otherwise noted $Q_A$ is fixed in the oxidized state for all $Q_B$ titrations and likewise the proximal $Q_B$ is fixed in the quinone state and $Q_{BD}$ deleted, for $Q_A$ titrations.

Look-up tables are calculated for electrostatic and non-electrostatic conformer self- and conformer-conformer pair-wise interactions. The electrostatic pair-wise interactions and reaction field energies are calculated by using the finite-difference technique to solve the Poisson-Boltzmann equation with the program DelPhi (*39, 42, 43*). Three focusing runs are done, giving a final resolution of 1.2 grids/Å (*44*). The protein is surrounded by water. The interior dielectric constant is 4 while 80 is used for the solvent with a salt concentration of 150 mM. The Lennard-Jones interactions are calculated using A and B parameters previously described (*13*). The possible microstates of the system are subjected to Monte Carlo sampling. A microstate is made up of one conformer for each residue, cofactor, and water. The energy of microstate n ($\Delta G^n$) is the sum of the electrostatic and non-electrostatic energies (*45*) (eqn. 2.6).

$$\Delta G^n = \sum_{i=1}^{M} \delta_x(i)\{\gamma(i)[2.3k_bT(pH - pK_{sol,i}) - nF(Eh - Em_{sol,i})]$$

$$+(\Delta\Delta G_{rxn,i} + \Delta G_{pol,i} + \Delta G_{nonel,i})\} + \sum_{i=1}^{M} \delta_x(i) \sum_{j=i+1}^{M} \delta_x(j)[\Delta G_{ij}^{el} + \Delta G_{ij}^{nonel}] \qquad (2.6)$$

$k_bT$ is 0.59 kcal/mol (25.8 meV), $M$ is the number of conformers, $\delta_x(i)$ is 1 for conformers that are present in the state and 0 for all others, $\gamma(i)$ is 1 for bases and –1 for

acids, and 0 for polar groups and waters, $n$ is the number of electrons gained or lost in redox reactions, $F$ is the Faraday constant, $pK_{sol,i}$ is the $pK_a$ of the ith group in solution. $E_{m,sol,i}$ is the midpoint potential of the ith cofactor in solution. $\Delta\Delta G_{rxn,i}$ is the difference between the conformer reaction field energy in solution and protein (desolvation energy). $\Delta G_{pol,i}$ is the pair-wise electrostatic interaction of a conformer with the backbone and with side chains that have no conformational degrees of freedom. For each conformer, Lennard-Jones interactions with the backbone and with all side chains with no degrees of freedom were summed and added to the torsion angle energy as $\Delta G_{nonel,i}$. $\Delta G_{ij}^{el}$ and $\Delta G_{ij}^{nonel}$ are the electrostatic and Lennard-Jones pair-wise interaction between each conformer in the microstate. The limits on the summation of the interconformer terms ensure that each interaction is counted once. Monte Carlo sampling establishes the Boltzmann distribution of different conformers of each residue at 25°C, providing the probabilities of the quinone reactant and product states at a given solution redox potential ($E_h$) and pH. Multi-flip (*46*) between closely coupled residues is implemented (*47*). The SOFT function is not used (*35*). Forty million steps of Monte Carlo sampling leads to convergence for the system with 449 residues, including waters, with conformational degrees of freedom. There are 3833 conformers to be sampled. For each reported $E_m$ three Monte Carlo runs were made and the results averaged. The average uncertainty in the conformer occupancy is ±0.04. The uncertainty of calculated $E_m$s is ±4 mV.

***Calculation of free energy of quinone reduction reactions.*** The free energy of quinone reduction or protonation reactions, ΔG, at a given pH and $E_h$ is:

$$\Delta G = 2.3mk_bT(pH - pK_a) - nF(E_h - E_m) = -2.3k_bT\log\frac{[P]}{[R]} \qquad (2.7)$$

where $F$ is the Faraday constant, $m$ and $n$ the number of protons and electrons transferred. $pK_a$ and $E_m$ are values for quinone in the protein. $[R]$ and $[P]$ are the occupancies of reactant and product calculated by Monte Carlo sampling given the microstate energies in eqn. 2.6. To determine the *in situ* $\Delta G$ for each reaction only conformers for given reactant and product redox states are sampled. For example, to determine $\Delta G$ for the reaction $Q_BH^- + e^- + H^+ \rightarrow Q_BH_2$ only conformers of $Q_BH^-$ and $Q_BH_2$ are allowed. $Q_A$ would be fixed in its oxidized form and no conformers of $Q_{BD}$ would be allowed in any sampled microstate. There are 4 conformers with different locations for the protons on $Q_BH^-$ and on $Q_BH_2$ (see Fig. 2.5). Their accepted occupancies are summed. The reaction free energy is divided into two terms.

$$\Delta G = \Delta G_{sol} + \Delta\Delta G_{protein} \qquad (2.8)$$

$\Delta G_{sol}$ is the reference free energy in solution at the given pH and $E_h$. This includes the contributions of the intrinsic quinone proton or electron affinity and the ability of the solvent to donate protons and electrons given the pH and $E_h$. Thus:

$$\Delta G_{sol} = 2.3mk_bT(pH - pK_{a,sol}) - nF(E_h - E_{m,sol}) \qquad (2.9)$$

$pK_{a,sol}$ and $E_{m,sol}$ are the quinone reference values in water (Fig. 2.6 and Table 2.1). $\Delta\Delta G_{protein}$ is the shift in the energy of reduction or protonation as the quinone is moved from water into protein (*23, 45*). It is calculated from:

$$\Delta\Delta G_{protein} = -2.3k_bT\log\frac{[P]}{[R]} - \Delta G_{sol} \qquad (2.10)$$

$\Delta\Delta G_{protein}$ is due to the changes in quinone $pK_a$ ($\Delta pK_{a,protein}$) and/or $E_m$ ($\Delta E_{m,protein}$). Thus:

$$\Delta\Delta G_{protein} = -2.3mk_bT\Delta pK_{a,protein} + nF\Delta E_{m,protein} \qquad (2.11)$$

As the $E_h$ titrations are carried out at pH 7 $\Delta\Delta G_{protein}$ is $nF\Delta E_{m,7}$. The $E_m$s and $pK_a$s calculated for the quinone in the protein are each viewed as the protein shifting the solution quinone behavior. Thus:

$$E_m = E_{m,sol} + \Delta E_{m,protein} \quad (2.12)$$

$$pK_a = pK_{a,sol} + \Delta pK_{a,protein} \quad (2.13)$$

For the proton independent half reactions ($Q + e^- \rightarrow Q^-$, $Q^- + e^- \rightarrow Q^{-2}$ and $QH + e^- \rightarrow QH^-$) $m$ =0 (eqn. 6), so $\Delta\Delta G_{protein}$ is simply related to the shift in $E_m$ in protein, $\Delta E_{m,protein} = \Delta\Delta G_{protein}/nF$ (*45*). When Monte Carlo sampling is carried to determine $\Delta\Delta G_{protein}$ for the proton coupled electron transfers (e.g. $Q + e^- + H^+ \rightarrow QH$) $\Delta\Delta G_{protein}$ includes contributions from both $\Delta pK_{a,protein}$ and $\Delta E_{m,protein}$.

Quinone $pK_a$s can be determined by Monte Carlo sampling as a function of pH (*35*). However, this will not predict the correct free energy of protonation at pH 7 because the protein ionization and conformation change with pH. The free energy of proton transfer reactions at pH 7 were obtained from the difference between the energy of the electron transfer and the coupled electron and proton transfer reaction closing the thermodynamic cycle (Fig. 3.1) (*48*). For example, the standard free energy of the protonation reaction $Q_B^- + H^+ \rightarrow Q_BH$ at pH 7 is the difference between the $\Delta G$ of $Q_B + e^- + H^+ \rightarrow Q_BH$ and $Q_B + e^- \rightarrow Q_B^-$. A $pK_a'$ value, the effective $pK_a$ calculated at pH 7, is then obtained from the pH where the $\Delta G$ would be zero if the protein remained as it is at pH 7.

$$pK_a' = 7 - \Delta G/RT \quad (2.14)$$

The half reactions $E_m$s and $pK_a'$s were obtained for the relevant quinone reactions in the three binding sites. The energy $\Delta G$ of a particular electron transfer such as from

$Q_A^-Q_B$ to $Q_AQ_B^-$ is then the difference of the redox potential $E_m(Q_A/Q_A^-)$ and $E_m(Q_B/Q_B^-)$ of the two quinones.

***Factors contributing to*** $\Delta G_{protein}$. In the continuum electrostatics analysis the free energy change due to the protein (eqn. 2.11) can be broken down into:

$$\Delta\Delta G_{protein} = (\Delta\Delta G_{rxn} + \Delta G_{pol} + \Delta G_{nonel}) + \Delta G_{res} \qquad (2.15)$$

All terms are changes in the free energy of reactant and product redox state of the quinone when it is moved from water to protein. $\Delta\Delta G_{rxn}$, $\Delta G_{pol}$ and $\Delta G_{nonel}$ are independent of the distribution of other conformers. $\Delta G_{res}$, calculated with eqn. 10 accounts for the changing interaction of the quinone with the protein as it undergoes the redox reaction, as well as the energy needed to keep the conformers in the rest of the protein in equilibrium with the quinone charge and protonation changes. Thus:

$$\Delta G_{res} = \Delta G_{res}^{Prot} + \Delta G_{Prot\rightarrow Prot*}^{red} = \Delta G_{Prot\rightarrow Prot*}^{ox} + \Delta G_{res}^{Prot*} \qquad (2.16)$$

If, for example the reactant is $Q_B$ and the product is $Q_B^-$, $\Delta G_{res}^{Prot}$ is the difference in interaction of the protein with $Q_B$ and $Q_B^-$ in the protein equilibrated around $Q_B$ (Prot) and $\Delta G_{Prot\rightarrow Prot*}^{red}$ the energy it takes to move the protein into the conformation equilibrated around $Q_B^-$ (Prot*). The reduction could also happen by the alternate path where first the protein is moved to the conformation equilibrated around $Q_B^-$ requiring $\Delta G_{Prot\rightarrow Prot*}^{ox}$ and then the quinone is reduced in the pre-prepared protein, Prot*, ($\Delta G_{res}^{Prot*}$). $\Delta G_{Prot\rightarrow Prot*}^{ox}$ is always unfavorable while $\Delta G_{Prot\rightarrow Prot*}^{red}$ is always favorable. $\Delta G_{res}^{Prot*}$ is always more favorable than $\Delta G_{res}^{Prot}$ because the price of rearranging into the protein equilibrated around the product has already been paid (see (*45*) for a more complete discussion).

**Figure 2.3.** Thermodynamic box for the redox reaction from [Q, Prot] to [Q$^-$, Prot*].

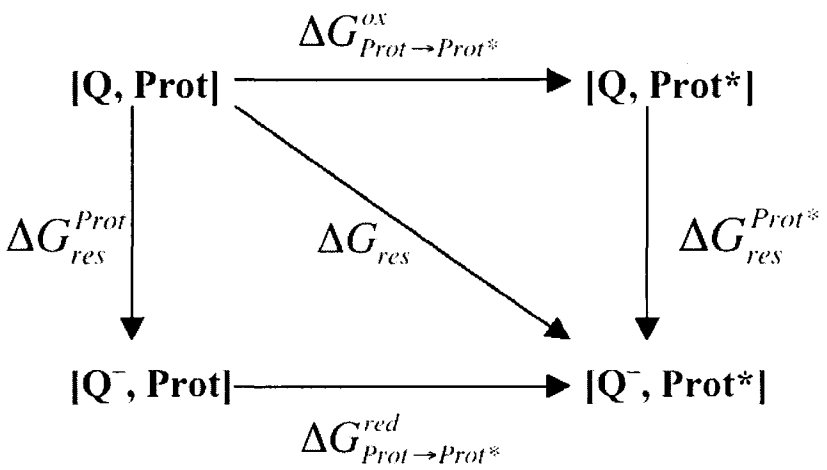


Diagonal $\Delta G_{res}$ is the outcome of MCCE calculations (eqn 2.15). Lower triangle: the quinone is reduced first in the oxidized, equilibrated protein ($\Delta G^{Prot}_{res}$); the oxidized protein relaxes to the reduced configuration ($\Delta G^{red}_{Prot \rightarrow Prot^*}$); Upper triangle: the protein is first changed to the conformation equilibrated in the reduced state keeping the quinone oxidized ($\Delta G^{ox}_{Prot \rightarrow Prot^*}$), the quinone is then reduced ($\Delta G^{Prot^*}_{res}$).

***Calculation of free energy difference for electron transfer.*** The free energy $\Delta G$ of a reduction reaction Reactant + $e^-$ → Product can be obtained from the $E_m$(Product/Reactant) multiplied by charge $q$:

$$\Delta G = qEm \tag{2.17}$$

Then the reaction energy $\Delta G$ of electron transfer from $Q_A^- Q_B$ to $Q_A Q_B^-$ can calculated as the difference of the redox potential $E_m(Q_A/Q_A^-)$ and $E_m(Q_B/Q_B^-)$ of the two quinones multiplied by one unit charge $q$:

$$\Delta G(Q_A^- Q_B \rightarrow Q_A Q_B^-) = q[Em(Q_A) - Em(Q_B)] \tag{2.18}$$

***Energy dynamics cycle closure.*** When carrying out more than one change of micro-system A → B → C, the free energies of $\Delta G(A \rightarrow B)$, $\Delta G(B \rightarrow C)$ and $\Delta G(C \rightarrow A)$ form a closed a thermodynamic cycle (*48*).

$$\Delta G(A \rightarrow B) + \Delta G(B \rightarrow C) + \Delta G(C \rightarrow A) = 0 \tag{2.19}$$

Then the free energy $\Delta G^0(A \rightarrow C)$ between initial and final states of a reaction chain can be calculated as the sum of two free energies of series reactions A →B followed by B → C, where B is a intermediate state.

$$\Delta G(A \rightarrow C) = \Delta G(A \rightarrow B) + \Delta G(B \rightarrow C) \tag{2.20}$$

For example, we can calculated the free energy of proton transfer reaction $Q_B^-$ → $Q_BH$ at pH 7 from the free energy difference of two electron transfer reactions $Q_B$ →$Q_BH$ and $Q_B$ →$Q_B^-$ at pH 7, which can be calculated with eqn. 2.7.

***Relative affinity ofdifferent quinone redox states***. The relative affinities of Q, $Q^-$ and $QH_2$ for the different quinone binding sites modulate the functions of bacterial RCs.

To the degree that the protein stabilizes the reactant or product state in an electron or proton transfer process, it will bind that species more tightly (Fig. 2.4) (*49*). For example, $\Delta\Delta G_{protein}$ for the $Q + e^- \rightarrow Q^-$ reaction can be used to compare the affinities of Q and $Q^-$ for the binding site,

$$\Delta\Delta G_{protein} = \Delta G_d^Q - \Delta G_d^{Q^-} = \Delta G_{protein}^{Q \rightarrow Q^-} - \Delta G_{sol}^{Q \rightarrow Q^-} = RT\left(\log K_d^{Q^-} - \log K_d^Q\right) \qquad (2.21)$$

where $\Delta G_d$ is the dissociation energy and $K_d^Q$ and $K_d^{Q^-}$ are is the derived dissociation constant for Q and $Q^-$, respectively.

**Figure 2.4.** Equilibrium dissociation energy ($\Delta G_d$) and redox energies of reaction.

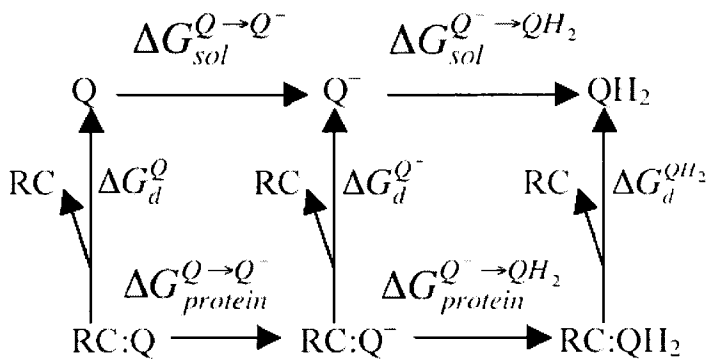


$\Delta G_d^Q$, $\Delta G_d^{Q^-}$ and $\Delta G_d^{QH_2}$ are the dissociation free energies for Q, $Q^-$ and $QH_2$.

## 2.3 Calculation models

### 2.3.1 Protein data files

The protein structure files 1AIJ(1AIG) (*2*), 1M3X (*3*), and 1PCR′ (*4*) with resolution of 2.2, 2.55, and 1.87 Å were analyzed. The three reaction center structures are very similar. The positions of the 12 residues with at lest an atom within 4.0 Å of the $Q_A$ quinone ring and 13 residues within 4 Å of the proximal $Q_B$ ring were compared. The backbone of 1AIJ has an RMS deviation of 0.12-0.13 Å with either 1M3X or 1PCR′. The side chain deviation is 0.5 Å for 1M3X and only 0.22 Å for 1PCR′. The $Q_B$ site shows larger changes. While the backbone varies by 0.17 Å between any of the structures, the side chains in 1A1J differ by 0.73 Å from 1M3X and 0.60 when compared with 1PCR′.

### 2.3.2 Ubiquinone Conformers

The positions of quinones were taken from PDB files 1AIJ and 1AIG (different coordinates of $Q_B$ in the inactive distal site and active proximal site). The hydroxyl proton position of semiquinone and dihydroquinone were placed at the four possible minimum energy positions $H_i$ (i=1,2,3,4) in Fig 2.5, all the hydroxyl protons are in the plane of the benzene ring. The length of the hydroxyl bond was 1.09 Å and the angle between the two possible nearby hydroxyl bonds was 60°. $H_1$ and $H_2$ are bonded at distal oxygen $O_5$, while $H_3$ and $H_4$ are bonded to proximal oxygen $O_2$. The semiquinone QH has four conformers with the hydrogen atom in one of the four possible hydroxyl positions ($H_1$, $H_2$, $H_3$ and $H_4$), and the dihydroquinone $QH_2$ also has four conformers with

the two hydrogens bonded to both $O_2$ and $O_5$ oxygen with combinations $H_1H_3$, $H_1H_4$, $H_2H_3$ or $H_2H_4$.

**Figure 2.5.** Four possible hydroxyl positions of quinone.

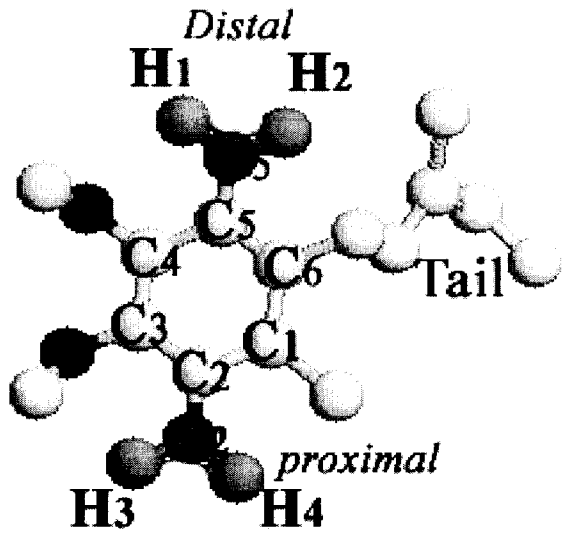

### 2.3.3 Redox potentials and $pK_a$s of quinones in solution

MCCE calculates the shift in free energy of a site redox or protonation reactions when it is moved from water into the protein, providing the changes in electrochemical midpoint, $E_m$, or $pK_a$. Given a reference solution $E_{m,sol}$ or $pK_{a,sol}$ for isolated cofactor, measurable values can be calculated (*45*). The redox midpoint potential of $UQ/UQ^-$ and $UQ^-/UQ^{-2}$ cannot be measured in aqueous solution at pH 7 because the $E_{m,sol}$ for quinone reduction to the semiquinone is lower than that for formation of the fully protonated dihydroquinone ($QH_2$). Thus, in water at physiological pH UQ is reduced in an n=2 reaction to $QH_2$ (*50, 51*). Estimates of the one electron reactions have been made for a small number of quinones in water (*52*). In the absence of protons the semiquinone is stable so $E_m$ measurements are far more straightforward. $E_m$s for $Q/Q^-$ have been determined in the aprotic solvent dimethylformamide (DMF) for a large number of quinones (*53*).

Several of the aqueous $E_{m,sol}$ for ubiquinones used here were estimated by comparison with the $E_m$s of tri- and tetra-methyl benzoquinones. UQ a 2,3-dimethoxy-5-methyl-6-isoprenyl-benzoquinone is considered to behave more like trimethyl than tetramethyl benzoquionone because the 2,3-methoxys cannot both lie in the plane of the ring so both cannot be electron donating as adjacent methyl groups can be (*53*). In DMF trimethyl benzoquinone has an $E_m$ for the half reaction $Q + e^- \rightarrow Q^-$ that is –30 mV more negative than UQ, while that of tetramethyl compound is 150 mV lower. The $E_m$ for the trimethyl semiquinone is –170 mV in water (*52*). An $E_{m,sol}$ for UQ of –145 mV, 30 mV more positive than trimethyl benzoquinone will be used here.

The $E_m$ ($Q/Q^-$) for ubiquinone in DMF was measured to be –360 mV (*53*). The value of –145 mV represents a shift of 215 mV moving from water to DMF as found for many small quinones (*54*). A pure Continuum Electrostatics analysis of the change in the Born reaction field energy on moving the Q to $Q^-$ reaction from DMF ($\varepsilon$=37) to water ($\varepsilon$=80) only predicts a shift stabilizing the anionic semiquinone by ≈40 meV, shifting the $E_{m,sol}$ to –320 mV (*25*). Thus, more specific interactions of water with the semiquinone not considered in the CE analysis shift the $E_m$ up.

The aqueous $pK_{a,sol}$ of semiubiquinone ($UQ^-/UQH$) was estimated to be 4.9 (*52*). Higher values of 6.5 are found in 80% ethanol-water(w/w) (*55, 56*). The $pK_a(QH^-/QH_2)$ of UQ was measured as 13.3 in 80% ethanol-water (w/w) (*55*). Using one possible correction of –1.6 pH units moving from 80% ethanol to water places the ubiquinone $pK_{a,sol}$ at ≈11.7, a high value given the electronegativity of the methoxy substitutents. Rather the aqueous, high pH trimethyl-BQ $pK_{a,sol}$ of 10.7 will be used here (*57*). The gap between $pK_{a,sol}(QH^-/QH_2)$ and $pK_{a,sol}(Q^{-2}/QH^-)$ is rather constant at 1.5~2 units (*56, 57*). This places the $pK_{a.sol}(Q^{2-}/QH^-)$ at 12.7 (*54*). Combining these $pK_a$s and the $E_{m,7}$ for $Q^- + e^- + 2H^+ \rightarrow QH_2$ of –360 mV (*54*) provides enough information to derive an $E_{m,sol}$ for $Q^- + e^- \rightarrow Q^{-2}$ of –195 mV as well as the other values in Table 1. The $E_m(Q^-/Q^{-2})$ for $UQ_0$ in DMF was measured to be –1080 mV (*53, 54*).

**Table 2.1.** Reference $E_m$s and $pK_a$s for ubiquinone-10.

| Half reactions | $pK_{a,sol}$ | $E°_{m,sol,7}$ (mV) | $\Delta G_{sol}$ [a] (meV) |
|---|---|---|---|
| $Q + e^- \rightarrow Q^-$ | - | –145[b] | 145 |
| $Q + 2e^- \rightarrow Q^{-2}$ | - | –170[b] | 340 |
| $Q^- + e^- \rightarrow Q^{-2}$ | - | –195[c] | 195 |
| $QH + e^- \rightarrow QH^-$ | - | 270[b] | –270 |
| $Q^- + H^+ \rightarrow QH$ | 4.9[d] | - | 124 |
| $Q^{-2} + H^+ \rightarrow QH^-$ | 12.7[f] | - | –338 |
| $QH^- + H^+ \rightarrow QH_2$ | 10.7[e] | - | –218 |
| $Q + e^- + H^+ \rightarrow QH$ | - | –269 | 269 |
| $Q + 2e^- + H^+ \rightarrow QH^-$ | - | 1 | –1 |
| $Q + 2e^- + 2H^+ \rightarrow QH_2$ | - | 220 | –220 |
| $Q^- + e^- + H^+ \rightarrow QH^-$ | - | 146 | –146 |
| $QH + e^- + H^+ \rightarrow QH_2$ | - | 488 | –488 |
| $Q^- + e^- + 2H^+ \rightarrow QH_2$ | - | 360 | –360 |

[a] $\Delta G_{sol}$ is $2.3mk_bT(pH - pK_{a,sol}) - nF(E_h - E_{m,sol})$ (eqn. 2.9) at $E_h$=0, pH=7, where $m$ is the number of protons and $n$ is the number of electrons; [b]By analogy with the $E_m$ of trimethyl-benozoquinone (*52*); [c] Derived from $E_m(Q/Q^-)$ and $E_m(Q^-/Q^{-2})$; [d] Derived from the $pK_{a,sol}$ for $Q^{-2}$ and the $E_{m,sol}$ for $Q^-$; [e] (*52*); [f] Derived from $pK_a(Q^{-2}/QH^-)$ being ≈2 units higher than $pK_a(QH^-/QH_2)$ (*54, 57*). Other values are derived as appropriate sums and differences walking around the thermodynamic box (Fig. 2.6). See Methods for a more complete derivation of $E_{m,sol}$s and $pK_{a,sol}$s used here.

**Figure 2.6.** Ubiquinone redox and protonation states.

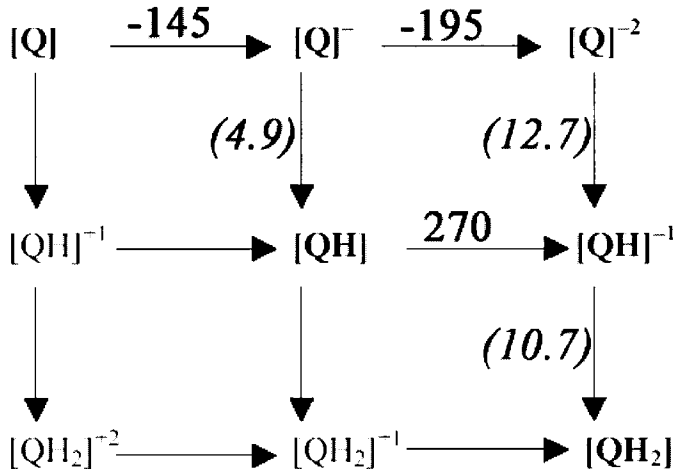


States in bold are intermediates considered in coupled electron (horizontal) and proton (vertical) transfer reactions in RCs. The sources for the $E_{m,sol}$ and $pK_{a,sol}$ (in parenthesis) are given in Table 2.1. The $\Delta G$ for proton transfer (vertical lines) at pH 7 can be obtained from $\Delta G = 59.3(pH - pK_a)$ (eqn. 2.14).

# Chapter 3 The energetic calculations of electrons and protons transfer reactions based on 1AIJ(1AIG) crystal structure

## 3.1 ABSTRACT

Multiple Conformation Continuum Electrostatics (MCCE) was used to study the ubiquinone electrochemical midpoints and $pK_a$'s for one and two electron reductions at the $Q_A$ and proximal and distal $Q_B$ sites in *Rb. sphaeroides* Reaction Centers based on crystal structure 1AIJ(1AIG). (1) At pH 7, the $E_m$ of $Q_A/Q_A^-$ is –40 mV and proximal $Q_B/Q_B^-$ –10 mV in reasonable agreement with experimental values. This assumes an $E_m$ of –145 mV in aqueous solution. $Q_B$ reduction requires significant changes in residue protonation and SerL223 reorientation in the $Q_B$ site. The $E_m$ for distal $Q_B/Q_B^-$ is –260 mV, so quinone can't be reduced here. (2) $Q_A$ and proximal $Q_B$ sites have similar interactions with Q and QH while in the distal $Q_B$ site the neutral semiquinone is favored. $Q_A$ and $Q_AH$ have similar interactions with the protein, while the distal $Q_B$ site favors the protonated semiquinone. (3) The $E_m$ for $Q^-/Q^{-2}$ is –700, –490, and –654 mV for $Q_A$, proximal and distal $Q_B$ ($E_m$ solution=–170 mV). In each site the dianion is very high in energy because the stabilizing interactions with residues and backbone increase with the charge (q) while the loss of solvation energy increases with $q^2$. (4) A pathway forming QH prior to the second reduction is prefered to forming the dianion in each site. $QH^-$ is at higher energy then $Q^-$ in both $Q_A$ and proximal $Q_B$ sites. (5) $QH_2$ is higher in energy at the $Q_B$ site than it is in solution so the reduced quinone binds poorly. In contrast, $QH_2$ is more stable than Q at the distal $Q_B$ site.

**Table 3.1.** MCCE calculated redox energies of quinone states.

| Half Reaction | # |
|---|---|
| $Q_B \rightarrow Q_B^-$ | A |
| $Q_B + e^- + H^+ \rightarrow Q_BH$ | B |
| $Q_B + 2e^- \rightarrow Q_B^{-2}$ | C |
| $Q_B + 2e^- + H^+ \rightarrow Q_BH^-$ | D |
| $Q_B + 2e^- + 2H^+ \rightarrow Q_BH_2$ | E |

(a) $Q_B$ proximal site

| Half Reaction | $\Delta\Delta G_{rxn}$ | $\Delta G_{pol}$ | $\Delta G_{nonel}$ | $\Delta G_{res}$ | $\Delta\Delta G_{protein}$ | $\Delta G_{sol}$ | $\Delta G_{calc}$ | $\Delta \log K_d$ |
|---|---|---|---|---|---|---|---|---|
| A | 386 | -389 | 0 | -135 | -138 | 145 | 7 | -2.4 |
| B | -15 | 74 | -23 | -43 | -7 | 269 | 262 | -0.1 |
| C | 1471 | -783 | 0 | -533 | 155 | 340 | 495 | 2.6 |
| D | 429 | -342 | -18 | -179 | -110 | -1 | -111 | -1.8 |
| E | 18 | 117 | -48 | -38 | 49 | -220 | -171 | 0.8 |

(b) $Q_B$ distal site

| Half Reaction | $\Delta\Delta G_{rxn}$ | $\Delta G_{pol}$ | $\Delta G_{nonel}$ | $\Delta G_{res}$ | $\Delta\Delta G_{protein}$ | $\Delta G_{sol}$ | $\Delta G_{calc}$ | $\Delta \log K_d$ |
|---|---|---|---|---|---|---|---|---|
| A | 317 | -219 | 0 | 19 | 117 | 145 | 262 | 2.0 |
| B | -20 | -16 | -8 | -15 | -59 | 269 | 210 | -1.0 |
| C | 1130 | -433 | 0 | -121 | 576 | 340 | 916 | 9.7 |
| D | 365 | -233 | -8 | -63 | 61 | -1 | 60 | 1.0 |
| E | 15 | -35 | -18 | 8 | -30 | -220 | -250 | -0.5 |

(c) $Q_A$ site

| Half reaction | $\Delta\Delta G_{rxn}$ | $\Delta G_{pol}$ | $\Delta G_{nonel}$ | $\Delta G_{res}$ | $\Delta\Delta G_{protein}$ | $\Delta G_{sol}$ | $\Delta G_{calc}$ | $\Delta \log K_d$ |
|---|---|---|---|---|---|---|---|---|
| A | 390 | -254 | 0 | -244 | -108 | 145 | 37 | -1.8 |
| B | -13 | 19 | -15 | -10 | -19 | 269 | 250 | -0.3 |
| C | 1479 | -494 | 0 | -588 | 397 | 340 | 737 | 6.7 |
| D | 430 | -219 | -16 | -8 | -13 | -1 | -14 | -0.2 |
| E | 18 | 13 | -21 | -12 | -2 | -220 | -222 | -0.03 |

MCCE calculations with quinone in proximal and distal $Q_B$ and $Q_A$ sites at pH 7 and $E_h$ 0 with P, the bacteriochlorophyll dimer, neutral. $\Delta G_{sol}$ ( $E_h$ 0, pH 7) is calculated as $2.3mk_bT(7-pK_{a,sol})-nF(0-E_{m,sol})$ (eqn. 2.9) using $pK_{a,sol}$ and $E_{m,sol}$ from Table 2.1. For protonated quinones, $\Delta\Delta G_{rxn}$ and $\Delta G_{pol}$ are the values for the four conformers with different proton positions weighted by their occupancies in Monte Carlo sampling (Fig. 2.5, Table 3.3). $\Delta\Delta G_{protein}$ calculated with eqn. 2.10; $\Delta G_{res}$ with eqn. 2.15. (a)The $pK_a$' ($pK_a$ calculated from the energy of protonation at pH 7) for $Q_B^-$ is 2.7, for $Q_B^{-2}$ is 17.3 and for $Q_BH^-$ is 8.0. (b)The $pK_a$' for $Q_{BD}^-$ is 7.9, for $Q_{BD}^{-2}$ is 21.4 and for $Q_{BD}H^-$ is 12.2. (c)The $pK_a$' for $Q_A^-$ is 3.4, for $Q_A^{-2}$ is 19.7 and for $Q_AH^-$ is 8.8.

**Table 3.2.** Energy of protein rearrangement on quinone reduction to semiquinone.

| Half reaction | $\Delta G_{res}$ | $\Delta G_{res}^{Prot}$ | $\Delta G_{res}^{Prot*}$ | $\Delta G_{Prot\rightarrow Prot*}^{red}$ | $\Delta G_{Prot\rightarrow Prot*}^{ox}$ |
|---|---|---|---|---|---|
| $Q_AQ_B + e^- \rightarrow Q_AQ_B^-$ | –135 | 86 | –318 | –221 | 183 |
| $Q_AQ_{BD} + e^- \rightarrow Q_AQ_{BD}^-$ | 19 | 69 | –74 | –50 | 93 |
| $Q_AQ_B + e^- \rightarrow Q_A^-Q_B$ | –244 | –263 | –279 | –19 | 35 |

$\Delta G_{res}$ calculated with eqn. 2.15. Other terms with eqn. 2.16. $\Delta G_{res}^{Prot}$ is the difference in interaction of the protein with quinone and semiquinone in the protein equilibrated around quinone (Prot) and $\Delta G_{Prot\rightarrow Prot*}^{red}$ the energy it takes to move the protein into the conformation equilibrated around the semiquinone (Prot*). The reduction could also happen by the alternate path where first the protein is moved to the conformation equilibrated around the semiquinone requiring $\Delta G_{Prot\rightarrow Prot*}^{ox}$ and then the quinone is reduced in the pre-prepared protein, Prot*, ($\Delta G_{res}^{Prot*}$) (see Fig. 2.3) (*45*).

**Figure 3.1.** MCCE calculated quinone redox energies in the three binding sites.

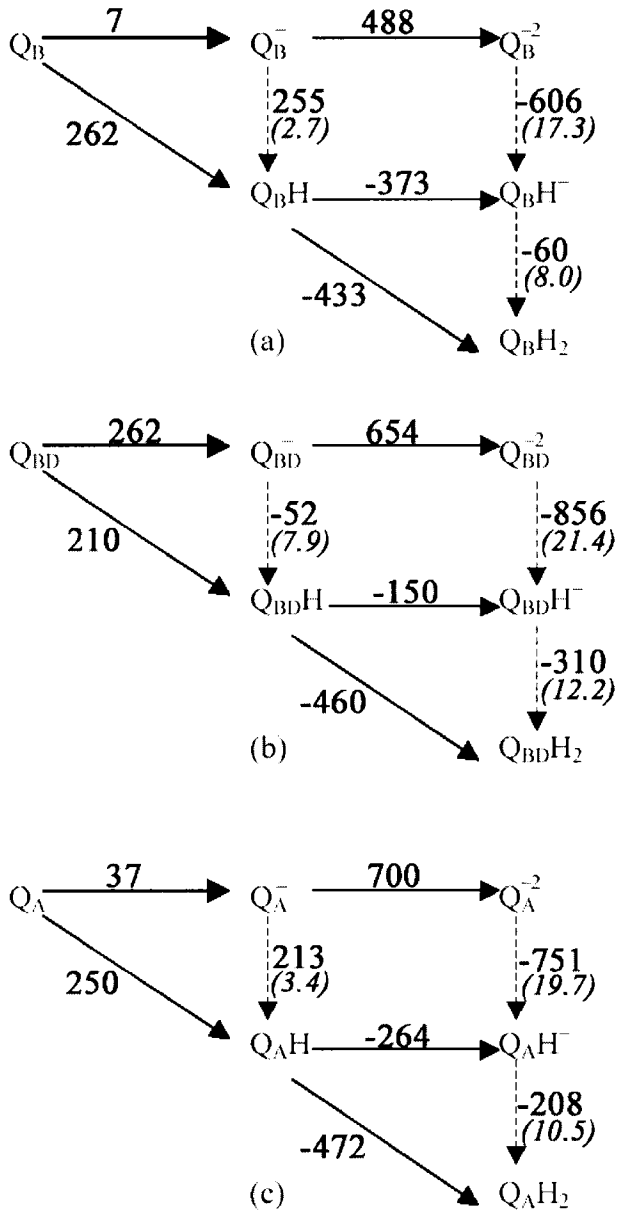


(a) $Q_B$ proximal site. (b) $Q_{BD}$ distal site. (c) $Q_A$ site. Horizontal arrows: Electron transfers; Dashed vertical arrows: Proton transfers; Diagonal arrows: Proton coupled electron transfers. ΔGs between all states connected by solid arrows were calculated by Monte Carlo sampling of reactant and product states as a function of $E_h$. ΔG of protonation reactions were obtained by closing the appropriated thermodynamic cycles. $pK_a'$ (in parenthesis) were obtained from the ΔG of protonation at pH 7 using eqn. 2.14.

**Figure 3.2.** Energy levels of quinone products in $Q_B$, $Q_{BD}$ and $Q_A$ sites.

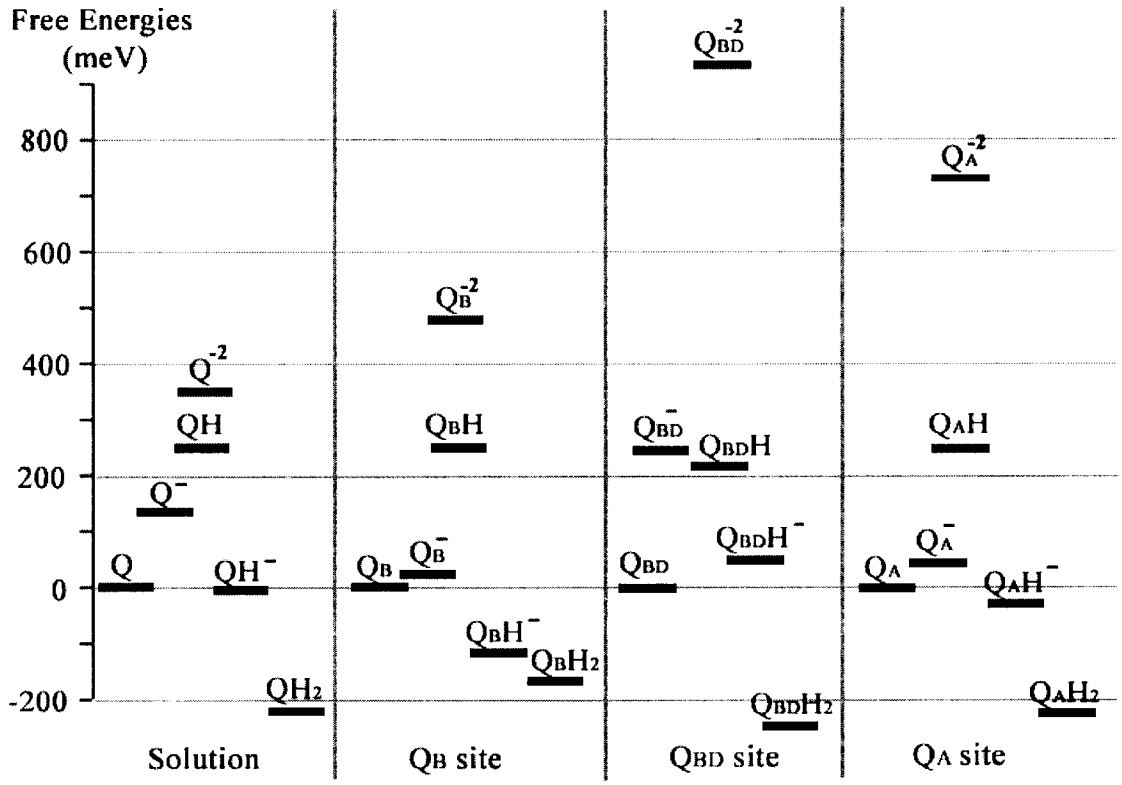


Values are from Table 3.1.

## 3.2 RESULTS

### 3.2.1. The energy of ubiquinone reduction at $Q_B$ proximal, $Q_B$ distal and $Q_A$ sites.

***The first reduction of $Q_B$ in the proximal binding site.*** The inner, proximal $Q_B$ site is calculated to stabilize quinone reduction to the anionic semiquinone by –138 meV relative to the same reaction in water ($\Delta\Delta G_{protein}$) (values are given to the nearest meV only as an aid to tracking the connections between the numbers). Using a solution reference $E_m$ ($E_{m,sol}$) of 145 mV (Table 2.1) the $E_m$ in the protein would be –7 mV (eqn. 2.12, Table 3.1a, 3.4a) in good agreement with the experimentally determined value of ≈30 mV (*58*). $\Delta\Delta G_{protein}$ can be divided into the loss of stabilization of the charge by water ($\Delta\Delta G_{rxn}$), the electrostatic pair-wise interactions with the protein backbone ($\Delta G_{pol}$) and the residues and ligands ($\Delta G_{res}$), and the short range Lennard-Jones interactions ($\Delta G_{nonel}$) (eqn. 2.15). $\Delta G_{res}$ includes the direct interactions between residues and the quinone as well as the energy required to change residue conformation and ionization states so they remain in equilibrium in each quinone redox state (eqn. 2.16, Table 3.2).

For the first $Q_B$ reduction, $\Delta\Delta G_{rxn}$ is ≈390 meV and $\Delta G_{pol}$ is ≈–390 meV, with the backbone dipoles essentially compensating for the removal from water (*24, 59, 60*) (Table 3.2). The primary contribution to $\Delta G_{pol}$ is from the residues L210 to 247 (helix E), with smaller contributions from the stretches M136-162 and M232-288. Pair-wise interactions with other side chains and ligands ultimately favor reduction by –140 meV (Table 3.1a). The +2 charge of the nearby non-heme iron provides a constant term favoring ionization of the proximal $Q_B$. However, other residues must undergo changes in ionization and conformation for $Q_B^-$ to be stabilized.

Monte Carlo sampling in MCCE maintains the ionization states and positions of surrounding residues in equilibrium with the quinone redox states. If the protein was fixed in the conformation and ionization equilibrated in the ground $Q_B$ state, $\Delta G_{res}^{Prot}$ is 86 meV (Table 3.2). Combining this with $\Delta\Delta G_{rxn}$, $\Delta G_{pol}$ and $\Delta G_{nonel}$ which are constant, yields $\Delta\Delta G_{protein}$ of 83 meV (eqn. 2.15). Adding the $E_{m,sol}$ of –145 mV yields an $E_m$ for $Q_B$ in the ground state protein of –228 mV indicating a very destabilized $Q_B^-$ (Table 3.2, eqn. 2.15). This is consistent with earlier calculations (*13*) as well as observation that in dark-adapted, frozen RCs $Q_B$ cannot be reduced by $Q_A$ (*61, 62*). It takes 183 meV to move the protein from the conformation equilibrated around $Q_B$ to one equilibrated around $Q_B^-$ without reducing the quinone ($\Delta G_{Prot\rightarrow Prot*}^{ox}$) (Table 3.2). Reduction in the pre-prepared protein would be stabilized by $\Delta G_{res}^{Prot*}$ to be very favorable. The resultant $E_m$ would be 318 mV. The calculated reaction $\Delta G_{res}$, –135 meV, is much less favorable (eqn. 2.16, Table 3.1a) because it includes the work to rearrange the protein from reactant to product conformation.

Proton uptake to surrounding residues, in particular GluL212 and AspL213 are the most important changes required to stabilize $Q_B^-$. As found in earlier calculations (*13*) a net charge of –1 is maintained on these 2 acids and $Q_B$. In these simulations when $Q_B$ is oxidized GluL212 is ionized and AspL213 protonated (Table 3.5). When $Q_B$ is ionized both acids are neutral. The orientation of the hydroxyl SerL223, which can offer a hydrogen bond to either AspL213 or $Q_B$ also changes on reduction (Table 3.3). The SerL223 conformers with the hydroxyls that are accepted by Monte Carlo sampling can donate a hydrogen bond to and accept a hydrogen bond from the neutral $Q_B$ (Table 3.3). When $Q_B$ is reduced SerL223 is a hydrogen bond donor to the anionic semiquinone.

***Protonation of the anionic semiquinone.*** The interaction of QH and Q with the $Q_B$ site are very similar (Table 3.1a). The ionization of the acidic cluster of GluL212 and AspL213 are the same (Table 3.5). The small differences in reaction field penalty is due to differences in the charge distribution in the two quinone species (*25*). The differences in Lennard-Jones interactions ($\Delta G_{nonel}$) and $\Delta G_{res}$ come from the interactions of the quinone proton with the protein. Three positions are acceptable with the majority of the quinones in Monte Carlo sampling donating a hydrogen bond to SerL223 (Table 3.3). The proximal $Q_B$ site is designed to stabilize anions, stabilizing $Q_B^-$ better than $Q_B$ or QH. The free energy of protonating $Q_B^-$ is 255 meV at pH 7 (Fig. 3.1). This would shift the quinone $pK_a'$ from 4.9 in solution to 2.7 in the protein (eqn. 2.14), so the quinone will remain deprotonated as is found.

***The second reduction of $Q_B$.*** The two-electron reduction of $Q_B$ is calculated to be 155 meV less favorable in the $Q_B$ site than in solution (Table 3.1a). $Q_B^{-2}$ is destabilized 1471 meV by $\Delta\Delta G_{rxn}$, $\approx$ 4 times that found for $Q_B^-$, while the favorable $\Delta G_{pol}$ is –783 meV, only twice that of the semiquinone. This is as expected given the continuum electrostatics linear response that underlies the calculations of the interaction of the static portions of the protein with the quinone charge. Thus, the pair-wise interactions for groups with no conformation or ionization changes double as the charge on the quinone doubles. However, the Born reaction field energy increases as $\approx q^2$ (*63*), so it costs 4 times more energy to bury a charge of –2 than –1. However, MCCE interactions with parts of the protein where change need not show a linear response to

changes in charge, such as GluL212 and SerL223. $\Delta G_{res}$ for $Q_B + e^- \rightarrow Q_B^-$ is much less favorable than $\Delta G_{res}^{Prot*}$, because work is done to modify the $Q_B$ site residues (eqn. 2.15, 2.16). However, there are only small changes in the position and ionization states of residues in the $Q_B$ site on the second reduction, Only GluH173 becomes partially protonated to stabilize the anion (Table 3.5) so little additional work is done to stabilize $Q_B^{-2}$. Thus, $\Delta G_{res}^{Prot} \approx \Delta G_{res}^{Prot*}$ for $Q_B^- + e^- \rightarrow Q_B^{-2}$ and $\Delta G_{res}^{Prot}$ for $Q_B^- + e^- \rightarrow Q_B^{-2}$ is approximately equal to twice $\Delta G_{res}^{Prot*}$ for $Q_B + e^- \rightarrow Q_B^-$. This illustrates how the resultant interaction of the quinone with the site, $\Delta G_{res}$, is largest when the site is pre-prepared ($\Delta G_{Prot \rightarrow Prot*}^{red} \approx 0$). However, even the added stabilization of the dianion due to the reaction occurring in a prepared protein is insufficient to pay the much larger reaction field penalty. If the $E_{m,sol}$ is –195 mV at $E_h$=0 the $E_m$ for the second reduction of the anionic quinone ($Q^- + e^- \rightarrow Q^{2-}$) is –488 mV.

***Protonation state of the doubly reduced $Q_B$.*** The singly protonated fully reduced quinone, $Q_BH^-$, is stabilized by –111 meV, interacting with the protein in a manner similar to that found for the semiquinone (Table 3.1a). The ionization states in the acidic cluster are the same as with $Q_B^-$ (Table 3.5). The $pK_a$ for binding the first proton to $Q^{-2}$ is 12.7 in solution. The $pK_a'$ is calculated to be pushed up to 17.3 in the $Q_B$ site because of the destabilization of $Q_B^{-2}$ (Table 3.1a, Fig. 3.1). The fully protonated, fully reduced $Q_BH_2$ is destabilized 49 meV by the protein. The interaction with the backbone ($\Delta G_{pol}$) in particular with the GlyL225 accounts for much of this unfavorable interaction. The $pK_a$ of $QH^-$ in solution is 10.7 but is only 8.0 in the protein, a reflection of the destabilization of the second bound proton.

**Figure 3.3.** Hydroxyl positions of SerL223 and $Q_B$ conformers.

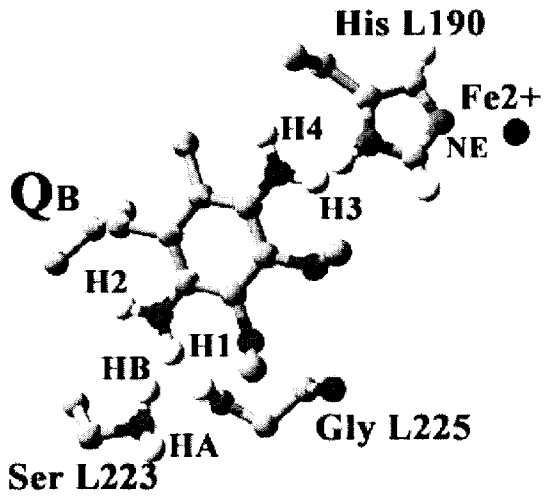


The UQ protons: H1, H2, H3 and H4. SerL223 protons: HA and HB. The side chain of the ligand HisL190 and the backbone of GlyL225 are also shown. The protein coordinates are taken from 1AIJ structure (*2*) with the quinone moved into the 1AIG proximal position as described in the methods section.

***Location of protons on $Q_B$.*** The quinone makes two hydrogen bonds in the $Q_B$ site. One is to HisL190, which lies between the non-heme Ferrous iron and $Q_B$. The other quinone carbonyl interacts with SerL223 and the backbone nitrogen of GlyL225. There are 4 positions for hydrogen sampled on $Q_B$ (Fig. 3.3). It can donate a hydrogen bond to (H1) or accept a hydrogen bond from (H2) SerL223 or, on the carbonyl proximal to the non-heme iron, it can point towards (H3) or away from (H4) HisL190. Two of the seven possible SerL223 conformers are occupied. In one it is a donor to AspL213 and can be a hydrogen bond acceptor from a protonated quinone (A), in the other it donates a hydrogen bond to $Q_B$ (B). When $Q_B$ is protonated the position of protons on the Ser and the nearby quinone carbonyl are correlated as expected.

In the $Q_B$ ground state the SerL223 donates a proton to $Q_B$ (B) with 80% probability (Table 3.3). This preference is strengthened in any of the anionic $Q_B$ states. The SerL223 hydroxyl in the A position destabilizes $Q_B^-$ by 67 meV while the hydroxyl in the B position stabilizes it by –114 meV. A better test of the importance of the SerL223 position can be gained by comparing the $E_m$ calculated with the Ser proton fixed, allowing the rest of the protein to come to equilibrium around each hydroxyl position. The $E_m$ with SerL223 B is –5 mV, essentially unchanged from that found in the free calculation. If the SerL223 is fixed in the A conformation, then the $E_m$ is lowered to –95 mV. Thus, as proposed previously (*64*) if the SerL223 is oriented to donate a hydrogen bond to AspL213 and not to $Q_B$ in the ground state, $Q_B$ reduction would be unfavorable.

In the neutral species $Q_BH$ and $Q_BH_2$, there is a distribution of quinone hydroxyl positions found in Monte Carlo sampling. It is somewhat more likely that the quinone

will be a proton donor to SerL223. However, different positions are found because there are several competing energy terms. No individual hydrogen bond between neutral $Q_B$ and SerL223 is very strong (<2 kcal/mol) so multiple orientations have similar energies. The only disallowed quinone proton position is the one that clashes with the hydrogen from HisL190 (H3). Thus, in $Q_BH$ H2, where the quinone accepts a hydrogen bond from SerL223, has a better interaction with backbone amide of GlyL225 and with SerL223 than H1, where the quinone donates a hydrogen bond to SerL223. However, H1 is found more often in Monte Carlo sampling because the correlated SerL223 position, HA, has a more favorable interaction with AspL213. In addition, there is room for a proton in the region near HisL190 on the other carbonyl (H4) and this position is sufficiently favorable that it is partially occupied in QH and $QH^-$. Favorable Lennard-Jones interactions with HisL190 ($\Delta G_{nonel}$) stabilize the proton.

***Relative affinity of the different redox states of quinone for the $Q_B$ proximal site.*** The difference in interaction of the quinone and another, product redox state with the protein is provided by $\Delta\Delta G_{protein}$ for that reaction (Table 3.1). The binding energies of the two species will also differ by $\Delta\Delta G_{protein}$ (Fig. 2.4, eqn. 2.21). For example, comparing $Q_B$ and $Q_B^-$, $\Delta\Delta G_{protein}$ is −138 meV indicating the semiquinone interacts 3.2 kcal/mol more favorably and will thus bind 220 times more tightly to the binding site. This is in agreement with experimental data showing $Q_B^-$ is more tightly bound then $Q_B$ or $Q_BH_2$ (*65*). $\Delta\Delta G_{protein}$ is similar for $Q_B^-$ or $Q_BH^-$ and so their relative affinities for the binding site will be similar. Again, since $\Delta\Delta G_{protein}$ is similar for Q and QH there will be little

different in these $K_d$s. For $Q_BH_2$ the $\Delta\Delta G_{protein}$ of 49 meV shows the dihydroquinone is more stable in solution, keeping $Q_BH_2$ 7 times less tightly bound than $Q_B$.

**Table 3.3.** Position of hydroxyl proton on SerL223 and proximal $Q_B$.

| Redox State | $Q_B$ | | | | SerL223 | |
|---|---|---|---|---|---|---|
| | H1 | H2 | H3 | H4 | A | B |
| $Q_B$ | – | – | – | – | 0.20 | 0.80 |
| $Q_B^-$ | – | – | – | – | 0.00 | 1.00 |
| $Q_B^{-2}$ | – | – | – | – | 0.00 | 1.00 |
| $Q_BH$ | 0.54 | 0.16 | 0.00 | 0.30 | 0.56 | 0.44 |
| $Q_BH^-$ | 0.08 | 0.72 | 0.00 | 0.20 | 0.07 | 0.93 |
| $Q_BH_2$ | 0.60 | 0.40 | 0.00 | 1.00 | 0.68 | 0.32 |

See Fig. 3.3 for hydrogen locations. Monte Carlo sampling carried out at pH 7 with the quinone redox state fixed.

***Redox reactions in the distal $Q_B$ site.*** There are multiple $Q_B$ binding sites found in X-ray crystal structures (*2, 5*). In wild-type RCs, two distinct $Q_B$ binding sites (distal and proximal to the non-heme iron) have been described. In the charge-separated $P^+Q_AQ_B^-$ structure (1AIG), the inner proximal semiquinone $Q_B^-$ is located ≈5 Å closer to $Q_A$ than it is in the dark-adapted $PQ_AQ_B$ outer, distal site (1AIJ) and has undergone a 180° propeller twist around the isoprene chain. In this outer site the quinone is making hydrogen bonds with IleL224 and AlaL186.

The energetics of quinone reduction and protonation at the distal site ($Q_{BD}$) were calculated using the original distal, quinone position in 1AIJ. The $E_m$ for the $Q_{BD} + e^- \rightarrow Q_{BD}^-$ half reaction is –262 mV while it is –7 mV in the proximal site (Table 3.1). The $Q_B$ site stabilizes the semiquinone anion by –138 meV while the $Q_{BD}$ site destabilizes it by 117 meV (Table 3.1). Comparing the two sites there is 80 meV less reaction field loss in $Q_{BD}$, but 180 meV less favorable $\Delta G_{pol}$ and 255 meV more unfavorable interactions with the rest of the protein. Interactions with residues in the protein equilibrated around the oxidized quinone, $\Delta G_{res}^{Prot}$, is less unfavorable in the distal than the proximal site because the quinone is further from the acidic cluster (Table 3.2). However, the relaxation around the reduced quinone, $\Delta G_{Prot \rightarrow Prot^*}^{ox}$, provides far less stabilization. As in the proximal site motions of SerL223 and protonation of GluL212 stabilize $Q_{BD}^-$. However, with an anionic semiquinone in the $Q_{BD}$ site GluL212 remains 70% ionized, destabilizing the anionic quinone by ≈90 meV (Table 3.1b, 3.5).

The energies of the other redox states of $Q_{BD}$ show that the distal site destabilizes anionic quinones, while the neutral protonated $Q_{BD}H$ and $Q_{BD}H_2$ are stabilized more than in the proximal $Q_B$ site (Fig. 3.1, 3.2). There is adequate room in the binding site to

protonate either carbonyl, although the position pointing towards the IleL224 HN is disallowed. $Q_{BD}^{-2}$ is 421 meV higher in energy than $Q_B^{-2}$. The desolvation penalty for the fully reduced quinone is smaller in the distal site, but the stabilizing interactions with backbone and other residues much smaller. In contrast the dihydroquinone is stabilized relative to solution by –30 meV in the distal site while it is destabilized by 49 meV in proximal site. Thus, $QH_2$ will be bound 3 times more tightly in the distal site than is the quinone (Table 3.1, Fig. 3.1).

***$Q_A$ redox reactions.*** In bacterial RCs, $Q_A$ is tightly bound to the protein, and the positions of $Q_A$ in all crystal structures are well defined. The quinone is making hydrogen bonds to HisL219 and the backbone of AlaM260. The protein stabilizes reduction of $Q_A$ by –108 meV relative to the quinone in solution (Table 3.1c). Given $E_{m,sol}$ for $Q/Q^-$ of –145 mV this results in an $E_m$ of –37 mV close to the measured values of –45 (*66*) to –75 mV (*58*) at pH 7. $\Delta\Delta G_{rxn}$ destabilizes the anionic semiquinone by 390 meV, the same as found in the proximal $Q_B$ site. Interactions with backbone dipoles stabilize reduction by 254 meV. The primary contributions are from amides M260-271, in the loop leading into and the first 10 residues of the E transmembrane helix. $\Delta G_{res}$ is –244 meV. Reduction of $Q_A$ is favored even in the protein equilibrated with the oxidized quinone ($\Delta G_{res}^{Prot}$) (Table 3.2), in agreement with the ability of the dark adapted, frozen protein to form $Q_A^-$ following activation of the RCs with light (*67*). $\Delta G_{Prot \rightarrow Prot}^{ox}$. is 35 meV showing there are only small rearrangement in the MCCE calculation. Several polar residues including Thr M261 and M222 and Tyr H40 rearrange their hydroxyl dipoles to stabilize the charge.

The resultant $\Delta\Delta G_{protein}$ of −108 meV indicates that $Q_A^-$ will be bound 72 times tighter than $Q_A$.

There are a variety of studies that suggest a linkage between $Q_A$ and $Q_B$ (*68, 69*). The $E_m$ for $Q_A$ is slightly less negative when $Q_B$ is reduced than when $Q_B$ is oxidized (Table 3.4a). The charge-charge interaction between $Q_A^-$ and $Q_B^-$ itself lowers the $E_m$ by ≈55 mV. However, neutralization of Glu L212 in the $Q_B$ site acidic cluster raises the potential by ≈62 mV. The resultant $E_m$ thus changed by only around 10 mV when $Q_B$ is reduced.

As in the proximal $Q_B$ site the $Q_A$ site stabilizes species with a −1 charge relative to neutral or doubly reduced forms of the quinone. Protonation of $Q_A$ is more favorable then $Q_B$ with a $pK_a'$ of 3.4. The site destabilizes the dianion by 397 meV (Table 3.1c), significantly more than does the $Q_B$ site. There is adequate room in the binding site to protonate either carbonyl although protonation of the carbonyl near AlaM260 is favored.

**Figure 3.4.** Electron and proton transfer reactions in bacterial RCs.

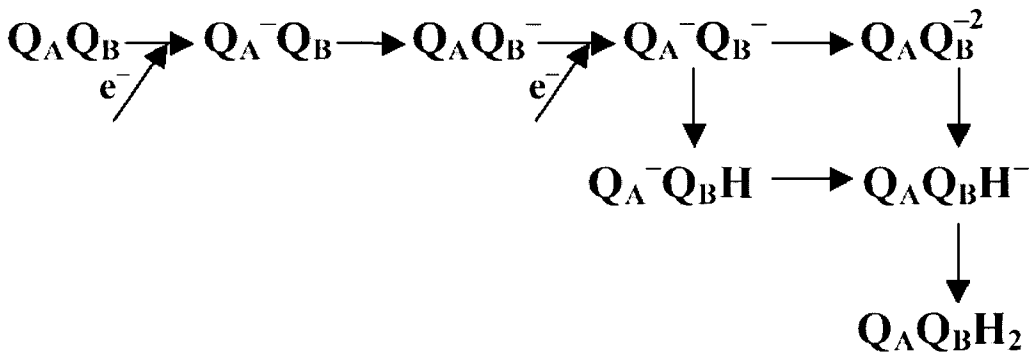


The free energy of the proton transfer $Q_A^-Q_B^- + H^+ \rightarrow Q_A^-Q_BH$ is calculated from the free energy difference between the reactions $Q_A^-Q_B^- + H^+ \rightarrow Q_AQ_BH^-$ and $Q_A^-Q_BH \rightarrow Q_AQ_BH^-$.

**Table 3.4.** Selected quinone half reactions calculated at pH 7.

| No | Half Reactions | $E_{m,sol}$ (mV) | $\Delta G_{sol}$ (meV) | $\Delta G_{protein}$ (meV) | $E_m$ (mV) | $\Delta G$ (meV) |
|---|---|---|---|---|---|---|
| 1 | $\mathbf{Q_AQ_B} + e^- \rightarrow \mathbf{Q_A^-Q_B}$ | –145 | 145 | –108 | –37 | 37 |
| 2 | $\mathbf{Q_A}\mathit{Q_B^-} + e^- \rightarrow \mathbf{Q_A^-}\mathit{Q_B^-}$ | –145 | 145 | –121 | –24 | 24 |
| 3 | $\mathbf{Q_AQ_BH} + e^- \rightarrow \mathbf{Q_A^-Q_BH}$ | –145 | 145 | –113 | –32 | 32 |
| 4 | $Q_A\mathbf{Q_B} + e^- \rightarrow Q_A\mathbf{Q_B^-}$ | –145 | 145 | –137 | –7 | 7 |
| 5 | $Q_A^-\mathbf{Q_B} + e^- \rightarrow Q_A^-\mathbf{Q_B^-}$ | –145 | 145 | –144 | –1 | 1 |
| 6 | $Q_A\mathbf{Q_B^-} + e^- \rightarrow Q_A\mathbf{Q_B^{-2}}$ | –195 | 195 | 295 | –490 | 490 |
| 7 | $Q_A\mathbf{Q_BH} + e^- \rightarrow Q_A\mathbf{Q_BH^-}$ | 270 | –270 | –103 | 373 | 373 |
| | | | | | | |
| 8 | $Q_A\mathbf{Q_B} + e^- + H^+ \rightarrow Q_A\mathbf{Q_BH}$ | — | 269 | –7 | — | 262 |
| 9 | $Q_A^-\mathbf{Q_B} + e^- + H^+ \rightarrow Q_A^-\mathbf{Q_BH}$ | — | 269 | –10 | — | 259 |
| 10 | $Q_A\mathbf{Q_B^-} + e^- + H^+ \rightarrow Q_A\mathbf{Q_BH^-}$ | — | –146 | 24 | — | –122 |
| 11 | $Q_A\mathbf{Q_BH} + e^- + H^+ \rightarrow Q_A\mathbf{Q_BH_2}$ | — | –488 | 56 | — | –433 |

**3.4(a):** The MCCE calculated redox midpoint potential of selected half reactions involving reduction of the proximal $Q_B$. The quinone which is undergoing the redox reaction is in bold type. If quinone is not changed, it is italicized.

| Reactions | Derived from | $\Delta G$(meV) | Exp. $\Delta G$ (meV) |
|---|---|---|---|
| $Q_AQ_B + e^- \rightarrow Q_A^-Q_B$ | $\Delta G_1$[a] | 37 | 45 (*66*) to 75 (*58*) |
| $Q_A^-Q_B \rightarrow Q_AQ_B^-$ | $\Delta G_4$-$\Delta G_1$ | –30 | –70 (*70-72*) |
| $Q_AQ_B^- + e^- \rightarrow Q_A^-Q_B^-$ | $\Delta G_2$[a] | 24 | 20 (*58*) |
| $Q_A^-Q_B^- \rightarrow Q_AQ_B^{-2}$ | $\Delta G_6$-$\Delta G_2$ | 464 | >240[b] |
| $Q_A^-Q_B^- + H^+ \rightarrow Q_A^-Q_BH$ | $\Delta G_9$-$\Delta G_5$ | 258 | 150 (*73*)[c] |
| $Q_AQ_B^{-2} + H^+ \rightarrow Q_AQ_BH^-$ | $\Delta G_{10}$-$\Delta G_6$ | –620 | >-215[b] |
| $Q_A^-Q_BH \rightarrow Q_AQ_BH^-$ | $\Delta G_7$-$\Delta G_3$ | –405 | --250±40 (*73*) |
| $Q_AQ_BH^- + H^+ \rightarrow Q_AQ_BH_2$ | $\Delta G_{11}$-$\Delta G_7$ | –60 | –90±18(*74, 75*)[d] |

**3.4(b):** Calculated free energy of electron and proton transfer reactions in bacterial RC. $\Delta$Gs derived from appropriate half reactions (Table 3.4a and Figure 3.4). [a] $\Delta$G calculated for reaction at $E_h = 0$ so $\Delta G = nFE_m$. [b] personal communication C. A. Wraight. [c] $\Delta$G at pH 7 derived from the estimated $\Delta$G of 180±30 meV at pH 7.5 (*73*). [d] $\Delta$G at pH 7 derived from the measured $pK_a$ of 8.5±0.3 (*74, 75*).

### 3.2.2. The energetics of the electron transfer reactions between $Q_A$ and $Q_B$.

***The first electron transfer:*** $Q_A^- Q_B \rightarrow Q_A Q_B^-$. In RCs, $Q_A$ is reduced forming $Q_A^- Q_B$, then the electron is transferred to $Q_B$ yielding $Q_A Q_B^-$ (Fig. 3.4). The MCCE calculated $E_m$s for $Q_A Q_B$ /$Q_A^- Q_B$ and $Q_A Q_B$/$Q_A Q_B^-$ half reactions are –37 and –7 mV (Table 3.4a). The free energy difference $\Delta G$ for $Q_A^- Q_B \rightarrow Q_A Q_B^-$ is –30 meV (Table 3.4b), close to the experimental results of ≈–70 meV determined from the rate of $P^+ Q_B^-$ charge recombination which proceeds via an equilibrated, thermal reduction of $Q_A$ (*70-72*). Any uncertainties in $E_{m,sol}$ for $Q/Q^-$ cancel in the calculated $\Delta G$. $Q_A$ and $Q_B$ are arranged with $c_2$ symmetry around the non-heme iron. The two sites have similar $\Delta\Delta G_{rxn}$. However, $Q_B^-$ has a much more favorable interaction with the backbone amide dipoles, $\Delta G_{pol}$, while $Q_A^-$ has a more favorable interaction with the residues of the protein (Table 3.1). The result is that following the rearrangements of the $Q_B$ site, the first electron transfer from $Q_A^-$ to $Q_B$ is favorable.

***The second electron transfer and subsequent protonation:*** $Q_A^- Q_B^- \rightarrow Q_A Q_B H_2$. The second electron transfer results in the state $Q_A Q_B H^-$ (Fig. 3.4) (*7, 75*). A mechanism where $Q_B^-$ is protonated forming $Q_B H$, followed by the second electron transfer is supported by the free energy and pH dependence of the rate of the second electron transfer from $Q_A^-$ to $Q_B^-$ (*76*). This conclusion is also supported by the analysis of the pH dependence of rhodoquionone (RQ) reduction in the $Q_B$ site. The $pK_a$ of RQ in solution is 7.3±0.2, binding a proton more tightly then UQ (*73*). The pH dependence of the rate of the second electron transfer shows that $RQ_B H$ is an intermediate when RQ is substituted for UQ. The free energy calculated here for $Q_A^- Q_B^- \rightarrow Q_A Q_B^{-2}$ of 464 meV

vs. $Q_A^-Q_B^-$ → $Q_A^-Q_BH$ of 258 meV supports the mechanism with proton transfer before electron transfer at pH 7 (Fig. 3.5). These results are also consistent with prior electrostatic calculations in *Rps. viridis* RCs (*77*).

The free energy change for $Q_A^-Q_B^-$ → $Q_A^-Q_BH$ was estimated to be 180 meV at pH 7.5 from a Marcus analysis comparing the electron transfer rates when RQ and UQ are in the $Q_B$ site (*73*). This would give a ΔG of 150 meV at pH 7 and a $pK_a'$ for $Q_B^-$ of 4.5. The calculated value for protonation of $Q_B^-$ is 258 meV, 110 meV less favorable than that derived from experiment. The calculated $pK_a'$ for $Q_B^-$ → $Q_BH$ is 2.7.

Kinetic measurements provide a free energy for the reaction $Q_A^-Q_B^- + e^- + H^+$ → $Q_AQ_BH^-$ of –70±10 meV at pH 7.5 (*75*), equivalent to a ΔG of –100 meV at pH 7. The free energy change for $Q_A^-Q_BH$ → $Q_AQ_BH^-$ would then be –250 meV. The value calculated here is –405 meV, significantly more favorable. One possible problem is that the $E_m$ for $Q_BH^-$ relies on the $E_{m,sol}$ for $Q^-/Q^{-2}$. A higher energy of $Q^{-2}$ would raise that of $Q_AQ_BH^-$, reducing the calculated ΔG between $Q_A^-Q_B^-$ and $Q_AQ_BH^-$.

Given the high energy of the $Q_AQ_B^{-2}$ state, the free energy difference between $Q_A^-Q_B^-$ and $Q_AQ_B^{-2}$ states is not measurable. The $E_m(Q_B^-/Q_B^{-2})$ has been estimated to be more negative than –240 mV (C.A. Wraight, personal communication). The calculated value is –464 mV. An experimental $pK_a$ limit of >10.7 was obtained for $Q_A^-Q_B^{-2}$ (*12, 78*). The calculated value is 17.3.

The $pK_a$ for $Q_AQ_BH^- + H^+$ → $Q_AQ_BH_2$ was estimated to be 8.5±0.3 from the steady-state proton uptake by $Q_B^{-2}$ (*74, 75*). This corresponds to a reaction free energy of –90±18 meV at pH 7 in agreement with the calculated value of –60 meV.

**Figure 3.5.** Calculated and experimental energy levels for doubly reduced states.

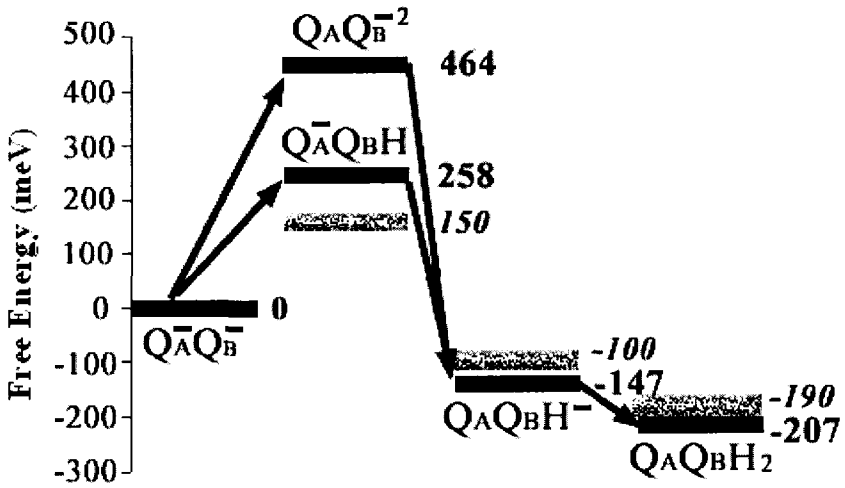


Solid lines: the MCCE calculated free energies (Table 3.4b); Gray lines: experimental from energy values (see Table 3.4b for details).

### 3.2.3. Charges in protanation of surrounding residues in different redox sites of the proximal $Q_B$

The MCCE calculated protonation and ionization states of several selected residues and the total proton uptake of protein at each immediate state of quinones $Q_A$ and proximal $Q_B$ at pH 7 are listed in Table 3.5.

In the electrostatic calculations, our calculated total proton uptakes at different quinones states are mainly dependent on the charges and their distributions on the quinones. When $Q_B$ is neutral, there are only a small total charges increase among the residues when compared with what is found in the ground state, for example $Q_AQ_BH$ and $Q_AQ_BH_2$ states. In the charged $Q_A$ redox states (as $Q_A^-Q_B$ and $Q_A^-Q_BH$ states), the total charge on the protein increases by around 0.15 $H^+$/RC, while it increases by 0.78 $H^+$/RC when the negative charge on $Q_B$ (as $Q_AQ_B^-$ and $Q_AQ_BH^-$ states). Structurally, $Q_B$ environments can allocated more protons than $Q_A$ environments since there are ionizable acids residues (AspL210, AspL213, AspM17 GluL212, GluH173) in $Q_B$ cluster. When the $Q_B$ is doubly reduced to $Q_B^{-2}$, the protein environment uptakes of 1.07 $H^+$/RC from solution in our calculations. The main contribution comes from GluL212 which takes around one proton. GluL212 is located in the interior edges of $Q_B$ binding pocket and proposed to be as the key residue to transfer the second proton to $Q_BH^-$ based on mutation experiments (*6, 7, 79*). GluH173 is also one of $Q_B$ cluster residues that strongly interact with $Q_B$ and is shown to play a role in the second electron transfer process by analysis of H173 Glu→Gln mutation (*79*).

HisH126 and HisH128 are located on surface of protein and had been shown to be the entry points and for first and second proton transfer to $Q_B$ by $C_d^{2+}$ and $Z_n^{2+}$ binding (*36, 80, 81*) and His →Ala site direct mutation (*82*). Our calculations find that the two His residues are partialy ionized and have small ionization changes in different quinone states. Although their conformational changes do not show up in this calculation, they are partialy ionized, which means smaller amount of energy is needed to change their ionization states. It is very possible that those two residues will change their charge states coupling with the quinone states changing.

**Table 3.5.** Protonation and ionization states of selected residues at pH 7.

| | $Q_AQ_B$ | $Q_A^-Q_B$ | $Q_AQ_B^-$ | $Q_A^-Q_B^-$ | $Q_AQ_B^{-2}$ | $Q_AQ_BH$ | $Q_A^-Q_BH$ | $Q_AQ_BH^-$ | $Q_AQ_BH_2$ |
|---|---|---|---|---|---|---|---|---|---|
| AspL210 | –1.00 | –1.00 | –1.00 | –1.00 | –1.00 | –1.00 | –1.00 | –1.00 | –1.00 |
| GluL212 | –1.00 | –0.98 | 0.00 | 0.00 | 0.00 | –0.97 | –0.77 | 0.00 | –0.93 |
| AspL213 | 0.00 | 0.00 | 0.00 | 0.00 | 0.00 | 0.00 | 0.00 | 0.00 | 0.00 |
| GluH173 | –1.00 | –1.00 | –1.00 | –1.00 | –0.97 | –1.00 | –1.00 | –1.00 | –1.00 |
| AspM17 | –1.00 | –1.00 | –1.00 | –1.00 | –1.00 | –1.00 | –1.00 | –1.00 | –1.00 |
| HisH126 | 0.70 | 0.70 | 0.66 | 0.65 | 0.63 | 0.70 | 0.69 | 0.65 | 0.69 |
| HisH128 | 0.43 | 0.42 | 0.43 | 0.43 | 0.43 | 0.44 | 0.43 | 0.43 | 0.43 |
| TOT | — | 0.15 | 0.78 | 1.01 | 1.07 | 1.00 | 1.25 | 1.76 | 2.00 |
| *Rb. sphaeroides* calculation (*26*) | — | 0.45 | 0.74 | — | — | — | — | — | — |
| *Rb. viridis* calculation[a] (*25*) | — | 0.14 | 0.60 | 0.88 | 0.97 | — | 1.15~ 1.14 | 1.68~ 1.65 | 2.01 |
| *Rb. viridis* calculation (*24*) | — | 0.58 | 0.60 | — | 2.10 | — | — | — | — |
| *Rb. sphaeroides* expt. (*83*) | — | 0.42 | 0.85 | — | — | — | — | — | — |
| *Rb. sphaeroides* expt. (*72*) | — | 0.34 | 0.39 | — | — | — | — | — | 2.1 |
| Rb. sphaeroides expt.[b] (*75*) | — | — | — | — | — | — | — | 1.1~1.4 | 2.0 |
| **Rb. capsulatus** expt. (*84*). | — | 0.31 | 0.58 | — | — | — | — | — | — |

Based on bacterial RC of *Rb. sphaeroides* structure 1AIJ(1AIG) and from previous calculations and experiments. [a] at pH 7.5 (*25*). [b] measured with Glu L212 → Gln mutation (*75*).

### 3.2.4. The influence of the membrane molecules outside the protein complex.

In nature, the bacterial RC proteins are embedded within a lipid membrane, and they function within the membrane. On the other hand, in the continuum electrostatic model, the boundary conditions of the protein configuration are important at the calculating of the electrostatic force field in the protein (*85*). So we set up the complex-membrane model for the continuum electrostatic calculation of pair-wise interactions. The influence of the membrane was estimated by including a shell of low dielectric material surrounding the protein. The dimension of the additional low dielectric constant region was 62x57x31Å, and the thickness of the membrane shell is at least 6Å to simulate the membrane lipid molecules. Then the calculated $E_m$s of $Q \rightarrow Q^-$ at $Q_A$ and proximal $Q_B$ with membrane are approximately 120 mV higher than the $E_m$s excluding the outside membrane. The effects of the outside membrane stabilize the semiquinone about hundreds of mV. Although there are shifts in calculating the free energies of quinone to semiquinone, the free energy of electron transfer between $Q_A^-$ and $Q_B$ reaction which is the difference of redox energies of $Q_A$ and $Q_B$ only shift about 10 meV (from –30 to –40 meV). In other words, the membrane will not change the free energy difference between $Q_A^-Q_B$ and $Q_AQ_B^-$ states too much.

**Fig 3.6.** The added artificial lipid membrane around RC crystal structures.

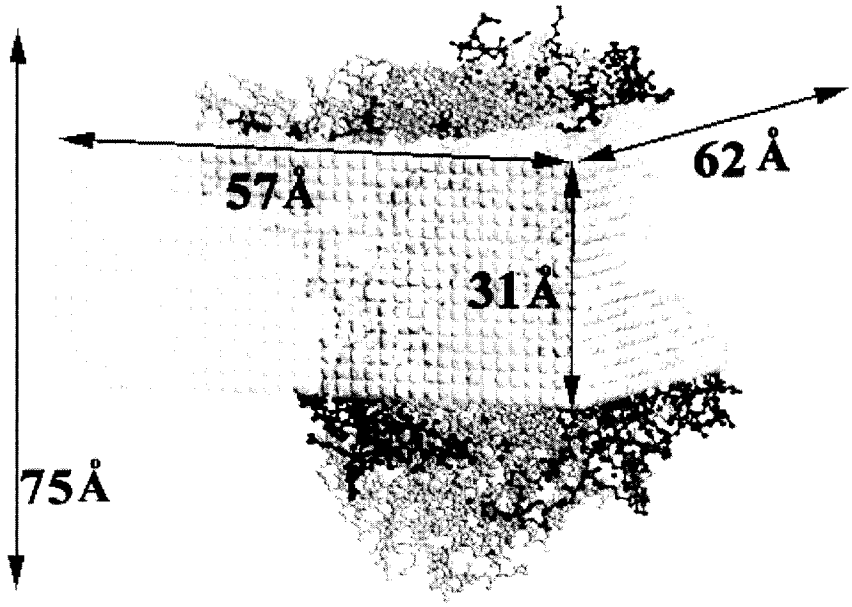

The quinones and non-heme iron cofactors are all embedded inside the proteins. The residues whose absolute electrostatic interactions with the proximal $Q_B^-$ are more than 25 meV must be near the $Q_B$ site. The added low dielectric membrane boundary conditions increase all those large interactions little. On the other hand, the residues that weakly interact with $Q_B^-$ without the membrane are far away from the $Q_B$ site, some of them are on the surface near the low dielectric lipid membrane region. The different boundary conditions would change the electrostatic interaction between them and $Q_B^-$. Those small interactions increase by as much as a factor of 3 upon addition of the membrane.

In the bacterial RCs structure, there are more negative ionizable residues than positive ionizable residues near the proximal $Q_B$. In the sphere centered at the $Q_B$ ring with a radius of 10Å, there are 6 Glu and Asp with only 3 Arg and Lys. Statistically the ionized residues near $Q_B$ produced a negative electrostatic potential at $Q_B$ site, while the other ionized residues outside of the $Q_B$ cluster sphere produced a positive potential at $Q_B$ site. After the low dielectric membrane region was added to the protein complex, the interaction between outside residues near the membrane and the semiquinone were increased, the added positive potential of long-range interaction would help to stabilize the semiquinone at the $Q_A$ and $Q_B$ sites.

## 3.3 DISCUSSION

### 3.3.1. The quinone energies in the three RC binding sites.

In RCs of *Rb. sphaeroides* and *Rps. viridis* three quinone binding sites are found in the x-ray structures (*2, 86-88*). The two quinones symmetrically arranged around the non-heme iron are clearly identified with functionally well characterized $Q_A$ and $Q_B$ (*5, 69, 89*). $Q_A$ is the first quinone reduced, accepting an electron from the bacteriopheophytin in ≈150 ns (*90*). On two turnovers $Q_A^-$ reduces $Q_B$ and then the $Q_B$ semiquinone with rates of ≈100 μs (*91, 92*) prior to $Q_B$ leaving the protein as dihydroquinone (*93*). The role of distal quinone site is not yet clear (*2, 94-97*). MCCE has been used here to see how the RC structure influences the free energy of the quinone redox states (Fig. 3.2) so that ubiquinone can carry out different functions in these sites (Fig. 3.2 and Table 3.1). Different states are stabilized so that in each site the appropriate reactions are energetically accessible. In addition, each quinone species has a different affinity for each binding site. For example, quinone comes and goes in $Q_B$ and $Q_{BD}$ sites. The connection between stabilization of a redox state and the relative affinity of different redox states shows the semiquinone does not bind to the $Q_{BD}$ site, but does not leave the $Q_B$ site (Fig. 2.4) (*98*).

***$Q_A$.*** $Q_A$, is reduced by the bacteriopheophytin anion which has a life time of only a few nanoseconds. Thus, this quinone never dissociates so that it is always ready to react (*49, 99*). $Q_A$ serves as a single electron acceptor, cycling between $Q_A$ and $Q_A^-$ without binding protons. The MCCE calculations show that the $Q_A$ site stabilizes only the semiquinone (Table 3.1). The calculated $E_m$, made assuming an $E_{m,sol}$ for ubiquinone

in water of –145 mV is –37 mV, in good agreement with the measured value of ≈–60 mV (*58, 66*). The protein interacts weakly with a proton on either carbonyl. The free energy of proton binding is 89 meV less favorable in the $Q_A$ site than in solution, lowering the semiquinone $pK_a'$ from 4.9 to 3.4.

***$Q_B$.*** In *Rb. sphaeroides* RCs $Q_A$ and $Q_B$ are both ubiquinones, which are modified by their binding sites so they can function differently. $Q_A^-$ lives for hundreds of milliseconds so $Q_B$ has time to bind to an empty site before $P^+Q_A^-$ returns to the ground state, which would waste the energy of the absorbed photon. $Q_B$ is thus twenty times more weakly bound than $Q_A$ (*49, 99*). $Q_B$ cycles through the $Q_B$, $Q_B^-$, $Q_BH$, $Q_BH^-$, and $Q_BH_2$ states during turnover, alternating reduction and protonation reactions. The proximal $Q_B$ site stabilizes the anionic states $Q_B^-$ and $Q_BH^-$ and interacts weakly or slightly unfavorably with the protonated neutral states $Q_BH$ and $Q_BH_2$. An important requirement for RC function is that $Q_A^-$ can reduce both quinone and semiquinone species within the ms lifetime of $Q_A^-$. Despite the $c_2$ symmetry of $Q_A$ and $Q_B$ sites in the protein, the $Q_B$ site stabilizes the semiquinone somewhat more that the $Q_A$ site does, in large part because of the larger positive potential from the backbone dipoles in the proximal $Q_B$ site. The free energy for the first electron transfer is modest, ≈–70 meV experimentally (*70-72*), –30 meV here, so $Q_B^-$ is not deeply trapped. This allows the electron to return to $P^+$ reforming the ground state via reduction of $Q_A$ with a half time of ≈1s if a second electron is not delivered to $Q_B$. The $Q_B$ site stabilizes $Q_BH$ little relative to solution (Fig. 3.1). This makes the $\Delta G$ between $Q_B^-$ and $Q_BH$ larger than it is in solution. However, the site destabilizes $Q_B^{-2}$ so $Q_BH$ not the dianion is the intermediate

for the second reduction of $Q_B$, in agreement with previous suggestions (*73, 80*). The $Q_B$ site stabilizes anions without a strong penalty for proton binding. This allows a favorable free energy for electron transfer from $Q_A^-$ to $Q_BH$ to form $Q_BH^-$. It is particularly important that the semiquinone species do not leave the $Q_B$ site before the second electron is delivered from $Q_A^-$. The –140 meV stabilization of $Q_B^-$ and –110 meV stabilization of $Q_BH^-$ ensures that these will bind more tightly to the $Q_B$ site than the quinone does. There is a modest, 50 meV, destabilization of $Q_BH_2$. This puts the energy of $Q_BH_2$ below that of $Q_BH^-$, but above that of $QH_2$ in solution, yielding favorable proton binding to $Q_BH^-$, but weak binding to the $Q_B$ pocket.

***$Q_{BD}$.*** RC crystal structures have shown that ubiquinone binds in several positions in the $Q_B$ site (*88*). X-ray crystal structures were compared of RCs frozen in the light and in the dark. In the dark-adapted structures, where the quinone was assumed to be oxidized, it was found in the outer distal site (*2*). In the light adapted structure, where the state was assumed to be $P^+Q_B^-$, the quinone is in the proximal site. The distal head group moves ≈5 Å out of the protein into a location overlapping the tail of a proximal quinone. In addition the two positions differ by a 180° rotation around the isoprene tail. Prior kinetic data had shown that the electron transfer from $Q_A^-$ to $Q_B$ is gated by a conformational change (*100*). The motion from proximal to distal binding sites was proposed as a good candidate for this rate determining step (*2*). However, several more recent experiments have cast doubt on this hypothesis. Recent time resolved crystallography in *Rps. viridis* (*96*) shows that only the proximal site is occupied at room temperature in ground and $P^+Q_B^-$ states of RCs that are undergoing turnover. This agrees

with FTIR studies that there are no changes in quinone position in active RCs (*94, 97*). Likewise the kinetic studies show that the tail has little effect on the electron transfer from $Q_A^-$ to $Q_B$, unexpected if the quinone needs to undergo rotation and translation in the rate determining step (*95, 99, 101*). The quinone position in crystals is sensitive to mutation (*102*) and temperature and cryoprotectant (*103*). Computational analysis has explored the transition from proximal to distal position showing there is little barrier to movement without (*20, 21*) and a large barrier with the 180° rotation (*19*). The protonation of the acidic cluster changes the relative affinity of the proximal and distal sites (*20, 21*). In addition, as is found here (Table 3.5) the proton uptake on $Q_B$ reduction depends on the quinone location (*104*).

MCCE analysis shows the distal $Q_B$ site ($Q_{BD}$) destabilizes all anionic quinone species while stabilizing the protonated neutral states (Fig. 3.1). Both $\Delta G_{pol}$ and $\Delta G_{res}$ are significantly less favorable than they are the $Q_B$ site. Reduction of $Q_{BD}$ to $Q_{BD}^-$ is ≈120 meV less favorable than it is in solution and 260 meV less favorable than in the proximal $Q_B$ site. Thus, $Q_A$ could not reduce $Q_{BD}$, so it is highly unlikely that electron transfer could occur to a quinone bound there. This is in agreement with prior calculations of RCs *Rps. viridis* (*25*). Earlier calculations on *Rb. sphaeroides* RCs show a 210 meV difference between reduction at the two sites, in good agreement with the values found here (*14, 27*). However, the neutral, protonated quinone species $Q_{BD}H$ and $Q_{BD}H_2$ are stabilized in the distal binding site. Thus, the dihydroquinone will be bound ≈3 times more tightly than the quinone to the distal site. It has been suggested that dihydroquinone, reduced during data collection, is the species found in the RC crystal $Q_{BD}$ site (*86*).

### 3.3.2. Comparisons with earlier experimental and computational studies.

The values have been presented to the nearest millivolt here as an aid for tracking the connections between values. However, neither the calculations nor the experimental data to which it is compared is known with this certainty. The uncertainty of the Monte Carlo sampling for this model of the RCs is less than 5 mV. MCCE analysis of benchmark $E_m$s (*45*) and $pK_a$s (*35*) provide show >90% of residues have an error of less than 60 mV or 1 pH unit. The calculations are sensitive to the starting crystal structures, parameters, and conformers (*34*). MCCE does not allow the backbone to change conformation and only limited side chain positions are sampled.

***Ionization of the acidic cluster.*** Perhaps the most difficult part of the simulation to define is the protonation state of the acidic cluster near $Q_B$ including GluL212, AspL213, AspL210 and GluH173 (Table 3.5). Their ionization states when the quinone is in the ground and $Q_B^-$ states have been the subject of many experimental (*69, 89, 105*) and computational studies (*13, 14, 26, 27*). Experiments, especially FTIR measurements have indicated that a partially deprotonated GluL212 becomes protonated when $Q_B$ is reduced (*11, 106, 107*). Simulations find that GluL212 and AspL213 are strongly coupled. Some studies find GluL212 is ionized (*14, 24, 26, 27*), others that AspL213 is ionized (*13, 21*), In calculations the pair usually have a net charge of –1 as they do here. When $Q_B$ is reduced GluL212 and AspL213 are always neutral, retaining a net charge of –1.

In the simulations starting with 1AIJ presented here when $Q_B$ is oxidized GluL212 is ionized (Appendix I). In parallel MCCE calculations carried out with 1M3X (*3*),

GluL212 is neutral and AspL213 ionized in the ground state (data not shown). This ease of shifting of the order of acid ionization arises because these two acids interact strongly so only one can be ionized and they have similar $pK_a$s in the absence of the interaction with each other so their ionization free energy is similar. Modest changes in the structure cause one or the other to be ionized first, keeping the other neutral to high pH. However, the $E_m$ for $Q_B$ differs by only 10 mV and the proton uptake is the same (0.7 $H^+/e^-$) in the simulations on 1AIJ and 1M3X. This is a result of the free energy of the reactant microstates with $Q_B$/L212$^-$/L213H and $Q_B$/L212H/L213$^-$ being very close together. The product state is always $Q_B^-$/L212H/L213H. This explains why the free energy of electron transfer from $Q_A^-$ to $Q_B$ in our earlier calculations where GluL212 was protonated and AspL213 ionized in the ground state differ by only ≈40 meV from those presented here (*13*). Similar clusters of acidic residues with coupled protonation are also found in bacteriorhodopsin (*47*).

***The importance of the membrane.*** While most measurements on bacterial RCs are carried out with detergent solubilized protein, RCs function in vivo embedded in the cell membrane. The reported reactions $E_m$s and $pK_a$s are somewhat dependent on the measurement conditions. For example, quinone $E_m$s are lower in chromatophores than in isolated RC (*108*). In contrast, preliminary calculations show that addition of a low dielectric slab to simulate the membrane (*85*) raises both the $Q_A$ and $Q_B$ semiquinone $E_m$s because there are more basic residues further from the quinones and more acidic residues nearby. Without the low dielectric slab the surrounding water screens the influence of the more distant positively charged groups. Experiments show addition of a few bound

cardiolipin molecules can lower the $Q_A/Q_A^-$ $E_m$ by –30 mV so at least some of the difference found in membranes may be due to the binding of specific lipids rather than the impact of dielectric screening by the membrane (*109*). Measurements provide a $\Delta G$ for electron transfer from $Q_A^-$ to $Q_B$ of ≈65 meV and ≈75 meV in chromatophores when P is neutral (*110*). In chromatophores the reaction is 45 meV more favorable when P is oxidized, indicating $P^+$ stabilizes $Q_B^-$ more than $Q_A^-$ (*110*). In contrast, the $\Delta G$ for electron transfer from $Q_A^-$ to $Q_B$ is relatively independent of the ionization state of P in isolated RCs (*71, 111*). The quinone $pK_a$s can also depend on the environment. Thus, experimental estimate for the $pK_a$ of $Q^- + H^+ \rightarrow QH$ is 4.5 in detergent solubilized RCs (*73*) and 6 in chromatophores (*108*).

***The role of SerL223.*** The position of the hydroxyl on SerL223 depends on the initial proton distribution on the acidic cluster in the $Q_B$ site. When AspL213 is neutral, as in these 1AIJ calculations, two hydroxyl positions are found in the Monte Carlo sampling so in the ensemble some SerL223 donate a hydrogen bond to and others accept a hydrogen bond from the neutral $Q_B$ (Table 3.3). However, if AspL213 is ionized when $Q_B$ is neutral, as it is in the 1M3X calculations, the hydroxyl of Ser L223 points to the Asp, away from $Q_B$. In both cases when $Q_B$ is reduced SerL223 serves as a hydrogen bond donor to the anionic semiquinone. The results presented here are in good agreement with a computational analysis that focused on the importance of SerL223 (*64*). The results presented here reaffirm the dependence of the Ser hydroxyl orientation of the charge of AspL213 and the approximate magnitude in the change in $Q_B$ $E_m$ if the Ser is fixed in one position or the other. If AspL213 is neutral when $Q_B$ is oxidized, the

conformations with different proton positions are close in energy and small changes in structure or fitting parameters could easily change the distribution. Thus, it seems likely that the Ser hydroxyl reorientation provides a significant barrier to electron transfer from $Q_A^-$ to $Q_B$ only if AspL213 not GluL212 is the member of the acidic cluster which is ionized when $Q_B$ is oxidized.

***The pathway of proton transfer to $Q_B$.*** Site-direct mutagenesis of Ser L223 suggests the first proton is transferred to the carbonyl from AspL213 via SerL223 and the second proton is transferred to oxygen near HisL190 through a pathway involving GluL212 (*7, 112, 113*). This is consistent with the first protonation being on the carbonyl near the SerL223 (Table 3.3). However in these calculations the proton on the carbonyl hydrogen bonded to HisL190, pointing away from the His NE2 hydrogen and the non-heme iron is found in 30% of $Q_BH$ (Fig. 3.3). This position has weak but favorable non-electrostatic interactions with both HisL190 and the non-heme iron. It may be that this proton can compete with protonation of the other carbonyl in equilibrium simulations, but would not be seen in RCs because protonation from the Ser is much faster.

***The importance of $E_{m,sol}$.*** The calculated $E_m$s vs. S.H.E. quinone $pK_a$'s and reaction $\Delta$Gs (Table 3.4) depend on the reference $E_{m,sol}$ and $pK_{a,sol}$ (*45*). As described in the methods section aqueous $E_m$s and $pK_a$s for ubiquionone have an uncomfortable number of uncertainties. Different errors for $E_{m,sol}$ for different half reactions will yield errors in calculated $\Delta$Gs. For example, the calculated free energy change for $Q_A^-Q_BH \rightarrow Q_AQ_BH^-$ is 150 meV more favorable than that estimated from measurements (Fig. 3.5)

(*75*). The calculated $\Delta G$ for the reaction relies on $pK_{a,sol}$ for $Q^{-2}$ and the $E_{m,sol}$ for reduction of the semiquinone as well as the calculated shift of the energy in the protein, $\Delta\Delta G_{protein}$. Errors in any of these terms will change the result.

Different analysis of RC electrochemistry have used different values for $E_{m,sol}$. For example, Knapp and coworkers (*14*) use –360 mV for the $E_{m,sol}$ for $Q/Q^-$ in dimethylformamide, a non-interacting reference solvent. In contrast, we prefer that all solution values are estimated in aqueous solution, as continuum calculations are optimized to determine transfers from water to protein. Thus, an $E_{m,sol}$ of –145 mV is used here, which is 215 mV more positive. The $E_m$s from (*14*) are reported to be more negative than those obtained here. However, their shifts in $E_m$ due to the protein actually favor $Q_A$ or $Q_B$ reduction to semiquinone by ≈100 meV more than those found here. The $\Delta G$ for the electron transfer between the two quinones is a value which is far less sensitive to the calculation. Calculated values at pH 7 range from –65 (*13*), to –60 (*14*), to –30 meV here. This is remarkable agreement considering the complexity of these calculations.

# Chapter 4 The role of clusters in the first electron transfer from $Q_A^-$ to $Q_B$ based on multiple X-ray structures of bacterial photosynthetic reaction centers

## 4.1 Abstract

X-ray crystallography has provided increasing detailed insights into the structures of the bacterial RCs, helping us understand how nature achieves highly efficient transformation of light electromagnetic energy to chemical energy. In three X-ray crystal structures of *Rb. sphaeroides* bacterial RCs, MCCE was used to calculate the redox midpoint potentials of $Q/Q^-$ at $Q_A$ and $Q_B$ proximal binding sites. At pH 7, the $E_m$s for $Q_A$ were calculated as –37mV(1AIJ(G)), –42mV (1M3X) and –27mV(1PCR′), the $E_m$s for $Q_B$ were calculated as –7mV (1AIJ(G)), 40mV (1M3X) and 40mV(1PCR′), which are close to the experimental data. Ionization states of $Q_B$ pocket residues such as AspL210, GluL212, AspL213 and GluH173 are different with neutral $Q_B$ in the different structures due to the small changes in positions of key residues. Therefore the MCCE calculated protein conformational changes upon the $Q_B/Q_B^-$ reaction in different structures are different. However, in MCCE simulations, each conformational change model gives the similar pH titration of the electron transfer free energy, which implies that despite different residues changing ionization upon $Q_B$ reduction the flexibility of the protein ensures the same proton uptake stables the changes at the $Q_B$ pocket.

## 4.2 Results

***The $E_m$ for reduction of $Q_A$.*** The $E_m$ for single electron reduction of $Q \rightarrow Q^-$ in water is estimated to be –145 mV (*54*), while the $E_m$ of $Q_A \rightarrow Q_A^-$ is calculated as around –35±7mV (–37mV in 1AIJ(G), –42mV in 1M3X and –27mV in 1PCR′). this indicates that the protein environment stabilizes quinone reduction by 100 mV. The semiquinone is destabilized by 400 meV by the loss of reaction field (solvation) energy as the quinone in moved from water into its binding site. The neutral quinone reaction field energy at the $Q_A$ site is about 100 meV and around 500 meV for the semiquinone. Interactions with the backbone dipoles stabilize reduction by 210~280 meV (Table 4.2). The primary contributions are from amides M260-271, in the loop leading into and the first 10 residues of the E transmembrane helix. Differences in the orientation of the C helix (L116-130) and E helix (L226-247) lead to the 33meV difference in $\Delta G_{pol}$ in the 1AIJ(G) and 1M3X (*1*).

MCCE maintains the ionization states and position of surrounding residues in equilibrium with the quinone redox states. However, the free energy of reduction can be calculated for a protein equilibrated around the oxidized (Prot) or the protein equilibrated with the reduced quinone (Prot*) (eqn. 2.16) (See Table 2.3 for a more complete discussion). Reduction of $Q_A$ is favorable even in the protein equilibrated with the oxidized quinone (Prot). This is in agreement with the ability of the dark adapted, frozen protein to form $Q_A^-$ following activation of the RCs with light. When the state [$Q_A^-$, prot] (reduced $Q_A$ with the protein fixed in the conformation equilibrated around the oxidized quinone) is allowed to relax the system [$Q_A^-$, prot*] is ≈30 meV lower in energy. In both 1AIJ(G) and 1M3X several polar residues including ThrM261 and

ThrM222 and TyrH40 rearrange their dipoles to stabilize the charge. There are some differences between 1AIJ(G) and 1M3X as they rearrange to stabilize quinone reduction. In particular, there is 0.2 $H^+$ bound per $e^-$ in 1AIJ and 0.49 in 1M3X (Table 4.3). The cluster of GluH38, GluH43, and GluH79 controls the difference. In both structures the net charge on the 3 acids is ≈–2.1 when the quinone is oxidized. However because of changes in side chain orientation, GluH79 is coupled to GluH43 in 1AIJ(G) and to GluH38 in 1M3X. The result is that in 1AIJ GluH38 remains fully ionized in both quinone redox states while there is some proton uptake by GluH79 on quinone reduction. In 1M3X GluH38 is much closer to its $pK_a$ in the ground state because of its interaction with GluH79. GluH38 is also the closest residue of the three to $Q_A$ and so is most influenced by quinone reduction, binding 0.58 protons. In both structures GluH43 transfers some its proton to protonate GluH38 or GluH79.

The $E_m$ for $Q_A$ is slightly more negative when $Q_B$ is reduced. The major factors are direct interaction with $Q_B^-$ itself (≈55 mV). However, neutralization of acidic residues in the $Q_B$ site raises the potential. As long-range interactions, in 1M3X neutralization of Asp raises the potential by 30 mV while in 1AIJ(G) GluL212 plays a larger role, raising the potential by ≈60 mV.

**Table 4.1.** Midpoint potentials and free energies of first electron transfer reactions in bacterial RC.

| | Reactions of first electron transfer | 1AIJ(G) | 1M3X | 1PCR′ | Ave. | Exp. |
|---|---|---|---|---|---|---|
| $E_m$ (mV) | $Q_AQ_B \rightarrow Q_A^-Q_B$ | –37 | –42 | –27 | –35±7 | –45 (*66*) to –75 (*58*) |
| $E_m$ (mV) | $Q_AQ_B \rightarrow Q_AQ_B^-$ | –7 | 40 | 40 | 24±27 | ≈30 to 20 (*58*) |
| $\Delta G^0$ (meV) | $Q_A^-Q_B \rightarrow Q_AQ_B^-$ | –30 | –70 | –67 | –56±22 | –70 (*70-72*) |

MCCE calculations at pH 7 based 1AIJ(G), 1M3X and 1PCR′ structures

**Table 4.2.** Energy terms for the primary quinone $Q_A$ and secondary quinone $Q_B$.

| Reactions | $Q_AQ_B \rightarrow Q_A^- Q_B$ | | | $Q_AQ_B \rightarrow Q_AQ_B^-$ | | |
|---|---|---|---|---|---|---|
| Based Crystal Structure | 1AIJ(G) | 1M3X | 1PCR′ | 1AIJ(G) | 1M3X | 1PCR′ |
| Experimental Free Energy (meV) | 45 (*66*) to 75 (*58*) | | | –30 to –20 (*58*) | | |
| $\Delta G_{sol}$ (meV) | 145 | | | 145 | | |
| $\Delta G_{calc}$ (meV) | 37 | 42 | 27 | 7 | –40 | –40 |
| $\Delta\Delta G_{protein}$ (meV) | -108 | –103 | –118 | –138 | –185 | –185 |
| $\Delta\Delta G_{rxn}$ (meV) | 390 | 403 | 403 | 386 | 381 | 391 |
| $\Delta G_{pol}$ (meV) | -254 | -208 | -282 | -389 | -360 | -390 |
| $\Delta G_{nonel}$ (meV) | 0 | 0 | 0 | 0 | 0 | 0 |
| $\Delta G_{res}$ [a] (meV) | -244 | –298 | –239 | –135 | –206 | –186 |

[a] $\Delta G_{res}$ calculated with eqn. 2.15.

**Figure 4.1.** The conformational changes upon the $Q/Q^-$ reaction of $Q_B$.

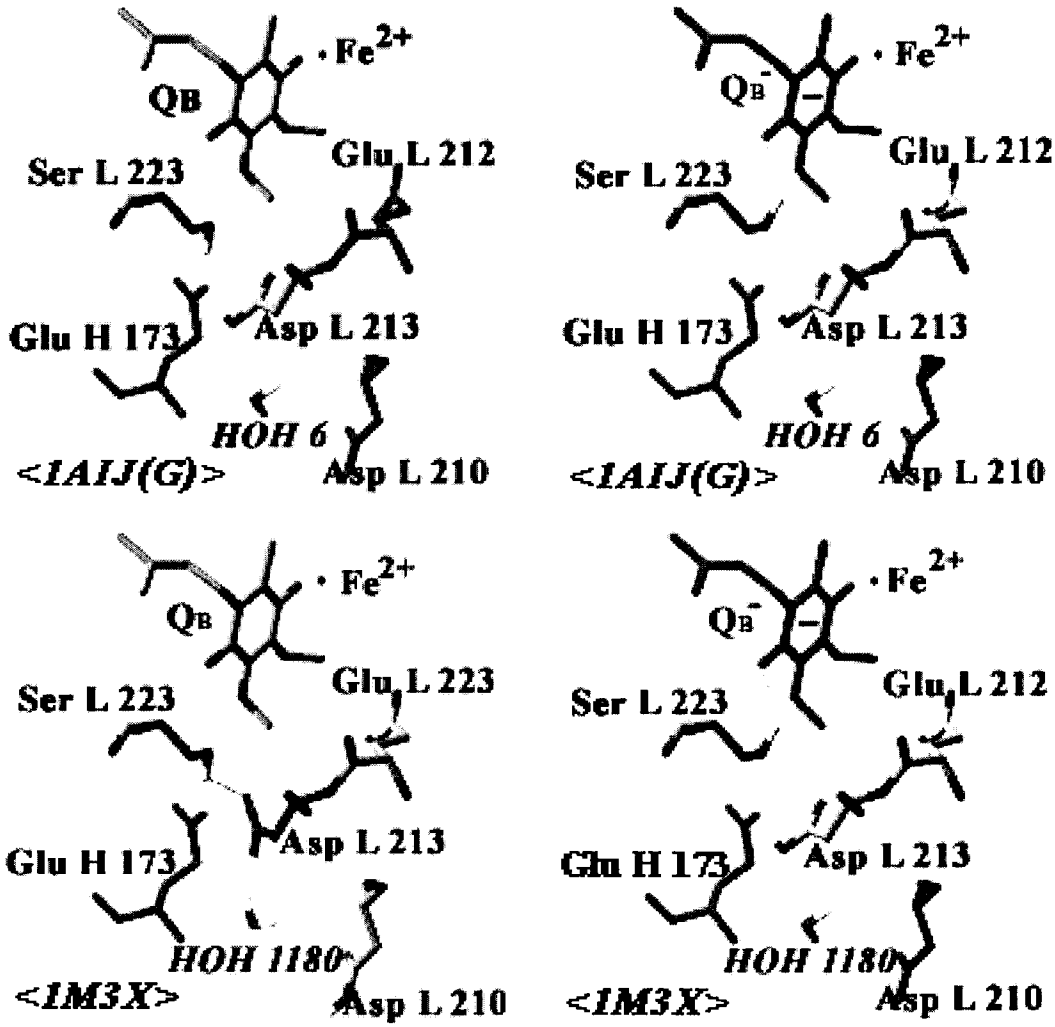


MCCE calculations based on 1AIJ(G) and 1M3X X-ray crystal structures. Red are oxygen atoms or negatively charged residues. Blue are nitrogen atom and green are hydrogen atoms.

***$Q_B$ reduction at proximal binding site.*** The $E_m$ for $Q_B \rightarrow Q_B^-$ is calculated to be 30 to 70 mV more positive than the $E_m$ of $Q_A \rightarrow Q_A^-$, in very good agreement with the experimental results. While the desolvation penalty is little different in the $Q_A$ and $Q_B$ sites, the interaction with the backbone is significantly (around 150 meV) more favorable in the $Q_B$ site (Table 4.2). $\Delta G_{res}$ is also quite different in $Q_A$ and $Q_B$ sites. In all proteins equilibrated in the ground or $P^+Q_A^-$ states the reduction of $Q_B$ ($\Delta\Delta G_{protein}$) would be unfavorable by ≈165 meV (Table 4.2). Significant rearrangement of the ionization states of the surrounding protein ($\Delta G_{res}$) stabilizes $Q_B$ by close to 200 meV(Table 2.4). This is consistent with earlier calculations (*13*) as well as the temperature dependence of the reduction of $Q_B$.

In each structure the groups that change protonation states on $Q_B$ reduction were identified. When $Q_B$ is neutral in 1AIJ(G) GluL212 is predominately ionized and AspL213 neutral. In 1M3X GluL212 is neutral and AspL213 ionized, Here SerL223 forms a hydrogen bond with $AspL213^-$, with the hydrogen of SerL223 and oxygen of AspL 213 separated by 2.63 Å. While in 1PCR′, GluL212, AspL213 and GluH173 are all partially ionized while AspL210 remains fully ionized (Table 4.3). In all proteins when $Q_B$ is ionized GluL212, AspL213 are neutral and GluH173 ionized, and SerL223 forms a hydrogen bond to the semiquinone $Q_B^-$. Thus, three different initial protonation states all provide similar $E_m$s for $Q_A$ and $Q_B$ reduction and similar free energies of $Q_AQ_B \rightarrow Q_AQ_B^-$ (Table 4.1). In those three different structures there are always three negative charges distributed among GluL212, AspL213, AspL210, GluH173 and $Q_B$ in the ground $Q_A^-$ and $Q_B^-$ states. In the ground and $Q_A^-$ states there is one proton in the acidic cluster, when $Q_B$ is reduced there are two.

**Table 4.3.** Changes of ionized $Q_B$ cluster residues.

| Struct. code | States | Calc. Proton uptake | Exp. Proton uptake | Charges on Glu L212 | Charges on Asp L213 | Charges on Asp L210 | Charges on Glu H 173 |
|---|---|---|---|---|---|---|---|
| 1AIJ(G) | $Q_AQ_B$ | 0 | 0 | **-1** | 0 | -1 | -1 |
| | $Q_A^-Q_B$ | 0.20 | 0.3~0.45[a] | **-0.96** | 0 | -1 | -1 |
| | $Q_AQ_B^-$ | 0.72 | 0.4~0.85[a] | **0** | 0 | -1 | -1 |
| 1M3X | $Q_AQ_B$ | 0 | 0 | 0 | **-1** | -1 | -1 |
| | $Q_A^-Q_B$ | 0.49 | 0.3~0.45[a] | 0 | **-1** | -1 | -1 |
| | $Q_AQ_B^-$ | 0.71 | 0.4~0.85[a] | 0 | **0** | -1 | -1 |
| 1PCR′ | $Q_AQ_B$ | 0 | 0 | **-0.62** | **-0.56** | -1 | **-0.76** |
| | $Q_A^-Q_B$ | 0.32 | 0.3~0.45[a] | **-0.40** | **-0.60** | -1 | **-0.73** |
| | $Q_AQ_B^-$ | 0.77 | 0.4~0.85[a] | **0** | **0** | -1 | -1 |

MCCE calculations results in 1AIJ(G), 1M3X and 1PCR′ X-ray structures. [a] The details of reference values of experimental are listed in Table 3.5

Table 4.4. Comparison of the energies of the $212^{-}213^{0}$ and $212^{0}213^{-}$ microstates in 1AIJ(G) and 1M3X structures by MCCE calculation.

| | 1AIJ(G) | | | 1M3X | | |
|---|---|---|---|---|---|---|
| **State** | **GluL212– AspL213°** | GluL212⁻ AspL213° | GluL212° **AspL213⁻** | **GluL212° AspL213⁻** | GluL212° AspL213⁻ | **GluL212⁻** AspL212° |
| Calc. methods | **Free** | *Virtual* | Fixed | **Free** | *Virtual* | Fixed |
| | | | | | | |
| Site 1 | **GluL212⁻** | AspL213⁻ | AspL213⁻ | **AspL213⁻** | AspL212⁻ | GluL212⁻ |
| GluM236⁻ | **-0.18** | *-0.09* | 0.10 | **0.93** | *1.86* | 1.86 |
| AspL210⁻ | **2.25** | *3.93* | 3.93 | **3.21** | *2.42* | 2.42 |
| SerL223 | **-0.22** | *0.17* | -2.51 | **-2.82** | *-0.19* | -0.14 |
| AsnM044 | **-0.14** | *0.80* | -1.38 | **-1.76** | *-0.23* | -0.14 |
| GluH173⁻ | **4.08** | *9.12* | 5.54 | **6.22** | *4.28* | 4.30 |
| Other Res | **-8.23** | *-9.06* | -8.97 | **-7.76** | *-8.96* | -9.24 |
| HOH | **-1.38** | *0.53* | 0.70 | **0.30** | *3.48* | -2.16 |
| $\Delta G_{res}$ | **-3.82** | *5.40* | -2.59 | **-1.68** | *2.66* | -3.10 |
| $\Delta G_{pol}$ | **-9.41** | *-8.00* | -8.00 | **-7.36** | *-8.39* | -8.39 |
| $\Delta\Delta G_{rxn}$ | **11.46** | *9.81* | 9.81 | **7.92** | *11.19* | 11.19 |
| $\Delta G_{nonel}$ | **-1.29** | *0.39* | 0.39 | **-1.53** | *-1.26* | -1.26 |
| $\Delta\Delta G_{protein}$ | **-3.06** | *7.60* | -0.39 | **-2.65** | *4.20* | -1.56 |
| $7 - pK_{a,sol}$ | **-2.25** | -2.25 | -2.25 | -2.25 | -2.25 | -2.25 |
| | | | | | | |
| Site 2 | **AspL213°** | GluL212° | GluL212° | **GluL212°** | AspL213° | AspL213° |
| $\Delta G_{res}$ | **-0.90** | *4.29* | -1.41 | **-2.03** | *2.73* | 1.33 |
| $\Delta G_{pol}+ \Delta\Delta G_{rxn}+ \Delta G_{nonel}$ | **1.48** | *0.53* | 0.53 | **0.50** | *1.32* | 1.32 |
| $\Delta\Delta G_{protein}$ | **0.58** | *4.82* | -0.88 | **-1.53** | *4.05* | 2.65 |
| | | | | | | |
| Site 1 & 2 States | **L212⁻&L 213°** | L212° &L213⁻ | L212° &L213⁻ | **L212° &L213⁻** | L212⁻ &L213o | L212⁻ &L213o |
| Energy | **-4.73** | 10.17 | -3.52 | **-6.43** | 6.00 | -1.16 |
| Difference | ref state | **14.90** | 1.21 | ref state | **12.43** | 5.27 |
| | | | | | | |
| ***GluL212*** | - | *5.39* | -0.26 | **-0.18** | - | - |
| ***AspL213*** | **0.42** | - | - | - | *4.85* | 0.10 |

The Free case (in bold type) is the MCCE free sampled protein environmental residues without fixing the ionization states of GluL212 and AspL213. The Virtual case (in italic

type) means specific ionization state of GluL212 and AspL213 with the MCCE free sampled protein environmental residues without fixing ionization states of GluL212 and AspL213. The Fixed case means MCCE sampled protein environmental residues with fixing ionization states of GluL212 and AspL213. All units in the table are in $\Delta pK_a$, 1 $\Delta pK_a$ units = 59.3 meV.

**Figure 4.2.** 1AIJ(G) and 1M3X structures difference.

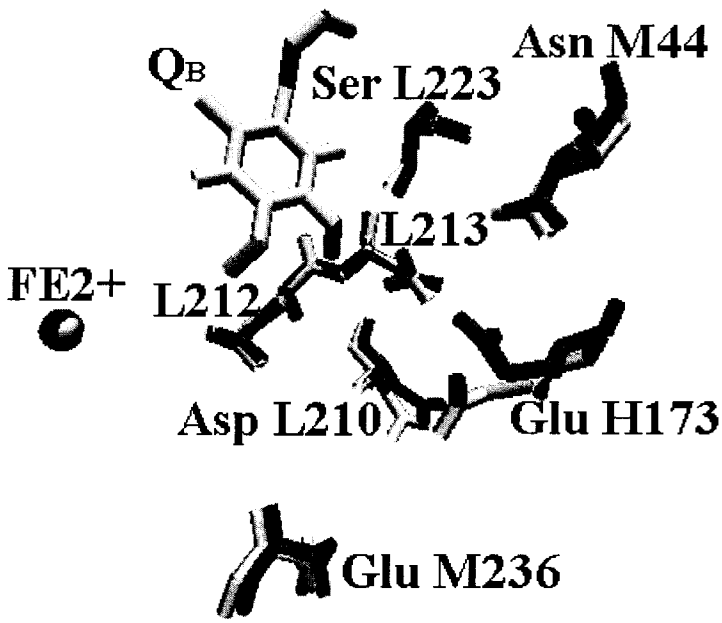


The structiures 1AIJ(G) and 1M3X were super-pasted by GluL212, AspL213 and FE atoms. 1AIJ(G) structure is in red and1M3X structure is in green.

***Why the ionization states are different in different crystal structures.*** There are only small differences in the structures that control the ionization behavior with the oxidized quinone. In particular, GluM236, AspL210, SerL223, AsnM44, GluH173 and several waters are keys to decide whether GluL212 or AspL213 will be ionized (Table 4.3). The influence of all other residues differs by less than 30 meV (0.5 $\Delta pK_a$ units) for ionization of the different residues.

From the Figure 4.2, it is clear that in 1AIJ(G) structure, SerL223, AsnM44 and GluH173 are closer to AspL213 than in the 1M3X structure. In 1AIJ(G) H173 is negatively charged and the polar AsnM44 and SerL223 are oriented with negative partial charges near AspL213, making AspL213 harder to ionized. Thus, in 1AIJ(G), ($L212^-L213^0$) is preferred. GluL212 ionization is also favored in 1AIJ(G) by GluM236 remaining neutral in all redox states. This residue is ionized in 1M3X and 1PCR′. Those small structure shifts makes $L212^-L213^0$ more stable in 1AIJ(G) and $L212^0L213^-$ more stable in 1M3X.

As has been described previously (*13, 24, 26-28, 77*) the acidic residues in the $Q_B$ site form a buffer where the net charge is relatively constant but the ionization states can vary with small changes in structure. The change in ionization is not well described by $pK_a$ shifts of individual residues as these describe the free energy of proton binding from water at a given pH. Here the relevant energies are that of the microstate with the same total charge but different site protonation. Relatively small changes in microstate energies can lead to stoichiometric proton shifts. That maintains the cluster net charge.

Table 4.4 compares the energies of the $212^-213^0$ and $212^0213^-$ microstates in 1AIJ(G) and 1M3X structures. In 1AIJ(G) $212^-213^0$ is the predominant state. A small

number of residues provide the major difference between the two sites. The other residues actually favor ionization of AspL213 slightly more than GluL212, while the backbone dipoles favor ionization of GluL212. The interaction of all protein side chains with $Asp213^-$ is 547 meV (9.22 $\Delta pK_a$ units) more unfavorable than with $GluL212^-$ in the equilibrium protein where $212^-213^0$ is the major state even without the consideration of the interaction with $Glu212^-$. Thus, $212^-213^0$ is 884 meV (14.9 $\Delta pK_a$ units) higher in energy than $212^0213^-$ in the equilibrated protein. A fairer measure of the free energy difference is to equilibrate the system with AspL213 forced to be ionized. Here the side chains and waters stabilize $AspL213^-$ by 154 meV (–2.59 $\Delta pK_a$ units). Reorientation of SerL223 and AsnM44, allow them to stabilize the fixed charge on $Asp213^-$. In addition, movement of GluH173 reduces its repulsion with the ionized Asp. Now the energy difference between $Glu212^-$ and $Asp213^-$ is 160 meV (2.7 $\Delta pK_a$ units). When the energy of the neural dipole is taken into consideration the difference between $212^-213^0$ and $212^0213^-$ is only 72 meV (1.21 $\Delta pK_a$ units). This provides an estimate of the energy difference of these two residues in these two microstates. The total microstate energies must also include the differences in the interactions amongst other residues in the protein equilibrated in the two states. For example, the different interactions between SerL223, AsnM44, and GluH173 are not accounted for.

The pattern for 1M3X is similar to 1AIJ(G). The same residues provide the bulk of the difference between the two states. Here the backbone dipoles stabilize the ionized $GluL212^-$ more than $AspL213^-$. However, here the loss of reaction field energy destabilizes $Asp213^-$ less. In addition, the protein favors the neutral $GluL212^0$ significantly more than it does $AspL213^-$. Several waters contribute to the difference in

energy of the neutral acids. Taken together the energy difference between $212^{0}213^{-}$ and $212^{-}213^{0}$ is 314 meV (5.3 $\Delta pK_a$ units).

The ionization states for 1PCR′ are more complex. The fraction ionization has 62% GluL212, 56% AspL213, and 76% GluH173 ionized with a total charge of -2.93. This is consistent with 40% of the RCs being found as $L212^{0}L213^{-}H173^{-}$, 33% as $L212^{-}L213^{0}H173^{-}$, 20% as $L212^{-}L213^{-}H173^{0}$ and 7% as the singly ionized $L212^{0}L213^{0}H173^{-}$. The energies of the four microstates were estimated by considering the interactions of the three cluster residues. The total energies are in reasonable agreement with the MCCE derived relative occupancies. The discrepancies are due to this calculation omitting changes in interactions amongst other residues that different in the different microstates. In addition, several conformers of each residue are occupied. The most occupied conformer is used in these mean field energy calculations. Thus, the mean field interaction of a single conformer of GluL212 is the occupancy-weighted average interactions with the MCCE distribution of conformers of AspL213 or GluL173. As in the other structures, SerL223 and AsnM44 change conformation to stabilize the different microstates. One difference is that GluM236 is neutral in the 1PCR′ calculations. In addition, the backbone and long-range interactions with other residues favor ionization of each acid while the interactions amongst the three acids destabilizes ionization.

**Figure 4.3.** pH titration curves of first electron transfer from $Q_A^-$ to $Q_B$.

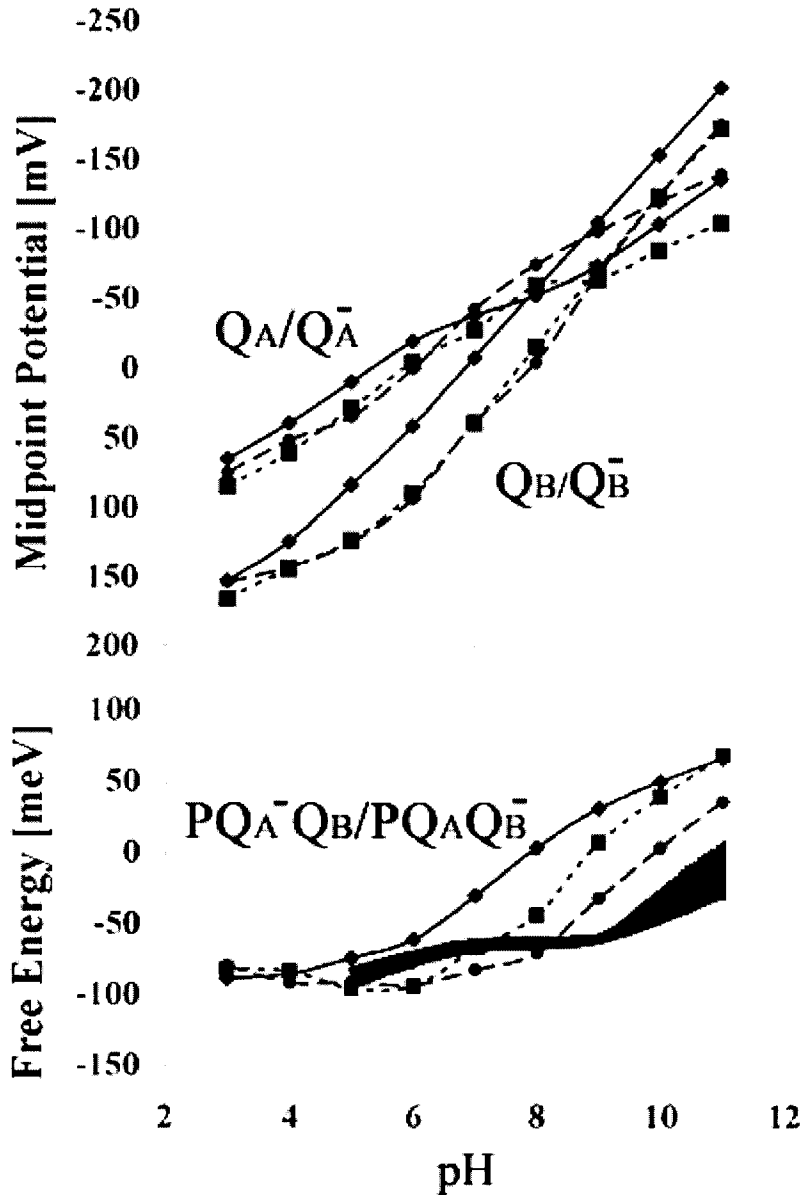


Based on MCCE calculations in bacterial RCs based on 1AIJ(1AIG), 1M3X and 1PCR´ crystal structures. Triangle linked lines are of 1AIJ(1AIG), circle linked lines are of 1M3X, and square linked lines are of 1PCR´.

***The pH dependence of electron tranfer from $Q_A^-$ to $Q_B$.*** The pH dependence of the quinone $E_m$s and resultant free energy of $Q_A^-$ to $Q_B$ electron transfer were determined (Fig 4.3). The experimental pH dependence of the free energy has a characteristic shape with the reaction being more favorable at low pH, with a relatively pH independent region from pH 6-9 with the reaction becoming less favorable at high pH. The calculated results show the same shape, however, the region of pH independence is shifted down ≈2 pH units.

The calculated free energy of $Q_A^-Q_B \rightarrow Q_AQ_B^-$ in 1AIJ(G) is about 50 meV higher than in 1M3X and 1PCR′ from pH 3 to pH 8. It is because that the calculated free energy of $Q_A \rightarrow Q_A^-$ in 1AIJ(G) is highest while the calculated free energy of $Q_B \rightarrow Q_B^-$ is lowest among these three cases except at high pH. There is a little difference in the $Q_A \rightarrow Q_A^-$ titration curves. Around pH 7, the slope of pH titration of calculated free energies of $Q_A \rightarrow Q_A^-$ based on 1M3X structure is a little bit higher (not too much) than in the other two cases. Around pH 7, reaction $Q_A \rightarrow Q_A^-$ takes up more protons than in the other two cases (because of the different role of GluH038).

Although the MCCE simulated conformation gating mechanisms for the first $Q_B$ reduction are different with different structures, they all uptake almost the same number of protons, and their pH titration curves of free energy of $Q_B \rightarrow Q_B^-$ are almost same (The differences within calculated $E_m$'s are all less than 50 mV).

## 4.3 Discussion

To understand how the protein environments modify the thermodynamic properties of quinone molecules at different binding sites, we calculated the midpoint potentials of $Q \rightarrow Q^-$ reactions at $Q_A$ and $Q_B$ proximal sites of bacterial RCs in the X-ray structures 1AIJ(G), 1M3X and 1PCR′ with MCCE method. The free energy $\Delta G^0$ of first electron transfer between $Q_A^-$ and $Q_B$ is calculated from the difference of $E_m(Q_A/Q_A^-)$ and $E_m(Q_B/Q_B^-)$ (eqn. 2.18). The conformational changes of $Q_B$ cluster residues upon the reduction of quinones at $Q_A$ and $Q_B$ sites are analyzed in detail. Different charge distributions among $Q_B$ cluster residues (GluL212, AspL213, GluH173 and AspL210) in the ground state were found in the calculations based on different X-ray structures. In the case of 1AIJ(G), GluL212 is protonated with 96% probability during the process of $Q_B$ reduction. While in the case of 1M3X structure, AspL213 is protonated during the $Q_B$ reduction. In those different cases, there are always three negative charges distributing among GluL212, AspL213, AspL210 and GluH173 and $Q_B$ during the process of the first electron transfer from $Q_A^-$ to $Q_B$. The difference is due to the small structural changes of some key residues around $Q_B$ site in different X-ray structures. Because the change of total charges distributed among the $Q_B$ cluster residues upon the first electron transfer between $Q_A^-$ to $Q_B$ is constant (near one), the curves of pH dependence of the redox potentials of $Q_A$ and $Q_B$ are almost the same in all cases.

***The polar energy stablized semiquinone at the $Q_B$ site.*** MCCE calculates the redox midpoint potential shift of a certain reaction, so a reference solution $E_m$ is required. The redox midpoint potential for ubquinone in solution is around –145 mV (*54*), which

means in water with external redox potential of zero, the neutral quinone is more stable than ionized semiquinone. Inside the protein, the redox midpoint potentials of the $Q_A \rightarrow Q_A^-$ and $Q_B \rightarrow Q_B^-$ were measured as −45 mV (*66*) and 30 mV (*58*). The question here is how a state that is very unfavorable in water is stabilized in the protein. In solution semiquinone is unstable, when the reaction moves from solution to protein, the reaction field penalty make $Q^-$ even unstable by around 400 meV. The calculations verified that the backbone energy (polar energy) stabilize the semiquinone by around 250 meV ($Q_A$ site) and 380 meV($Q_B$ site), and the +2 charged and ligands stabilizes the semiquinone by around 430 meV.

The MCCE calculation explored why the $E_m$ of $Q/Q^-$ in $Q_A$ site is around 30~70mV lower than in $Q_B$ site. Despite the fact that $Q_A$ and $Q_B$ are chemically identity, the asymmetry of the redox properties of $Q_A$ and $Q_B$ can only be the result of the asymmetry of their different protein environments. Based on the three different X-ray structures, we calculated the redox midpoint potential of $Q_AQ_B \rightarrow Q_A^-Q_B$ as around −35±7mV, the redox midpoint potential of $Q_AQ_B \rightarrow Q_AQ_B^-$ as 24±27 mV. To understand how the protein environment modifies the dynamic and energetic properties of quinones at $Q_A$ and $Q_B$ sites, MCCE breaks the energy into several terms. Each energy term adds to total microstate energy (see eqn. 2.15) was listed and compared in Table 4.2. In the $Q_B$ site, the difference of backbone energies $\Delta G_{pol,q}$ of $Q_B$ and $Q_B^-$ is about 140 meV more favorable than in the $Q_A$ site, which mainly decides that the free energy of $Q/Q^-$ in the $Q_B$ site is lower than in the $Q_A$ site. At $Q_A$, the neutral quinone is still more stable than the semiquinone at Eh=0, while energy gap of $Q_A/Q_A^-$ is reduced by around 100 meV by the protein environment. The energy gap of $Q_B/Q_B^-$ is reduced to make the semiquinone

more stable than the neutral quinone. Thus, the first electron can transfer from $Q_A^-$ to $Q_B$ for the energetics favors the $Q_AQ_B^-$ state rather than $Q_A^-Q_B$ state.

***The total negative charges around $Q_B$ is constant although different ionization configurations.*** In those three different structures, there are always three negative charges distributed among GluL212, AspL213, AspL210, GluH173 and $Q_B$ during the process of first electron transferring from $Q_A$ to $Q_B$. The mobile protons may be stabilized on GluL212 or AspL213 or both of them with some on GluH173 when $Q_B$ is neutral. After $Q_B$ reduction, both residues AspL213 and GluL212 are fully protonated. It is the reason why the proton-uptake upon the quinone reduction and $E_m$ vs pH behavior in three different X-ray structure simulations are almost same although their ionization states of $Q_B$ cluster residues are different in each case. Whatever the ionization states of the $Q_B$ cluster residues are, the free energy of first electron transfer from $Q_A^-$ to $Q_B$ is constant in the pH range 4 to 7.

Our MCCE calculations show that the ionization states of the $Q_B$ cluster residues are sensitive to the coordinates. In this region, most of the $Q_B$ cluster residues are protonable acids that can accept or transfer a hydrogen atom, and all of them can form strong or weak hydrogen bonds to their neighbors. The $Q_B$ cluster is much more flexible than the residues in $Q_A$ neighborhood. The MCCE calculations based on different X-ray structures give different charge distributions on GluL212, AspL213 and GluH173 in the $Q_B$ neutral state, in 1AIJ(G) structure $L212^0L213^-H173^-$ is energetically favoriable, in 1M3X structure $L212^-L213^0H173^-$ is energetically favoriable and in 1PCR′ there are mixture states of $L212^0L213^-H173^-$, $L212^-L213^0H173^-$, and $L212^-L213^-H173^0$. That

means in protein the energy levels of those microstates are designed to be very close, with energy gaps of only couple of $\Delta pK_a$ units. Small structural change can influence the energetic order of those microstates. The small changes of some residue positions in the X-ray structure 1AIJ(G), 1M3X and 1PCR′ yield different ionization states of $Q_B$ cluster residues in our MCCE calculation. GluL212, AspL213 and GluH173 surrounding residues work together as a charge buffer to stabilize the buried charges in $Q_B$. Since the protein is a dynamic system, if the lowest microstate is inhibited for some reason, another candidate state can be arranged to guarantee that the electron can always stabilized on $Q_B$ site. This kind of protein design broadens the energy level scheme of final $Q_B^-$ state, and increases its entropy. A buffer of a cluster of strongly interacting acids has also been found in other membrane proteins such as K-channel ion, cytochrome c oxidase (*114*) and bacteriorhodopsin (*47, 115-117*). The clusters may be a motif in molecular design to stabilize the reaction on the cofactors.

***Protein relaxations upon the reduction of quinone.*** In the point view of continuum electrostatics, there are two ways to stabilize a negative charge within protein: reorientation of surrounding dipoles, as in dielectric relaxation; and increasing or redistributing charges among the environmental residues. In photosynthetic RCs, upon the reduction of $Q_B + e^- \rightarrow Q_B^-$, the semiquinone at $Q_B$ site is stabilized by a conformational changes of the $Q_B$ cluster SerL223, GluL212, AspL213, GluH173 and some water molecules. There is a dipole reorientation of SerL223 to stabilize $Q_B^-$ by forming a hydrogen bond to the O1 carbonyl oxygen of semiquinone. And there are three

residues (GluL212, AspL213 and GluH173) that together take up one hydrogen to stabilize $Q_B^-$, although which residue get the hydrogen varies in our three calculations.

A rigid protein whose residue positions are fixed with a low, uniform dielectric constant 2, 4 or 6 and surrounded by water with a dielectric constant of 80 is often a standard continuum electrostatic model for the residue $pK_a$ and cofactor $E_m$ calculations (*34*). The calculations on bacterial RCs based on this mode without multiple conformers did not produce the favorable free energy to facilitate the first electron transfer between $Q_A^-$ and $Q_B$, i.e., this electron transfer is unfavorable (*13, 26*). In some $pK_a$ calculations, a higher dielectric constant of protein is needed to reproduce experimental results (*118*). The high apparent values suggests that specific conformational changes near ionizable residues can generate a highly effective, local dielectric response. This can be approximated by a uniform, high internal dielectric constant in that region. The Delphi calculations by assigning a high dielectric constant 20 in $Q_B$ region and 4 in the rest of the protein showed that high dielectric effectively stabilizes $Q_B^-$ compared with the same calculations of using an uniform protein dielectric constant 4 (*43*). However, this simple approach provides no microscopic information about the source of motion. In contrast, the multi-conformation method retains the distinction between regions of the protein where ionization produces large changes in the protein ($Q_B$ region) and sites that generate little dielectric response ($Q_A$ region). And MCCE gives a more precise simulation of protein dielectric response than the common continuum electrostatic model. Here the effective dielectric constant distribution in the protein depends on the geometry of backbone and amino acids type. In addition, the move of dipoles can be identified, and the ionization states of residues and cofactors in each reaction states can be calculated.

All the micro-motions (dipole and hydroxyl reorient direction and charge redistribution) can be called a dielectric response, and they contribute to the increase the effective dielectric constant in the calculations.

***Comparison with the results from experimants.*** There are site-direct mutation studies on bacterial RCs which show that GluL212 has a high $pK_a$ 9.0~9.5 while AspL213 has $pK_a$ below than 7, neutral pH within the $Q_B$ state, GluL212 is neutral and AspL213 is ionized. The pH-dependence of light-induced voltage changes (electrogenic events) (*119*) and the pH-dependence of proton uptake (*6, 12*) with wild-type, GluL212→Gln and AspL213 →Asn mutations assign a $pK_a$ value of around 9.5 to GluL212 and 4.5 to AspL213. Results of electron transfer rate measurements of site-direct mutations of GluL212 and AspL213 also can also be explained with the Asp predominantly ionized and Glu predominately protonated (*120*).

Infrared spectroscopy can also provide direct information about the residues that are involved in the first electron transfer from $Q_A^-$ to $Q_B$ (*121, 122*). There is one IR band that charges with the first reduction of $Q_B$ which is missing in the GluL212 to Gln mutant, but it present when AspL213, AspL210 and GluH173 have been mutated. It was proposed that at pH 7 GluL212 is partial ionized in the ground state and fully protonated with $Q_B^-$, AspL213 and GluH173 are always ionized (*106, 123, 124*). Recently, GluL212 is confirmed as the main proton acceptor in the state $Q_AQ_B^-$ by rapid-scan FTIR difference spectroscopy (*11, 106, 107*).

Our calculations based on 1AIJ(G) and 1M3X X-ray structures show that either GluL212 or AspL213 ionized and the calculation based on the 1PCR′ X-ray structure

choose a mixture. Whether the GluL212 or AspL213 was ionized at the $Q_B$ neutral state is very sensitive to the relative coordinates of environmental residues. In the protein, those two conformational gating residues (GluL212 and AspL213) can shift by the small coordinates shifts of the environmental residues. This may explain the contradictory experimental results gave the opposite results about the ionization state of GluL212 and AspL213 when $Q_B$ is neutral.

***Comparison with previous computations.*** The electron transfer from $Q_A^-$ to $Q_B$ in bacterial RC from *Rhodobacter sphaeroides* and its coupling to conformational changes has been the subject of several earlier theoretical studies by continuum electrostatic model calculations based on 1AIJ(G) X-ray structures (*13, 14, 26-28*).

Beroza et al. (*26*) used standard continuum electrostatic model for the $pK_a$ of acids residues that interact most strongly with $Q_B$. Water molecules were removed, hydroxyl protons were minimized in the protein ground state, and only ionization states of acidic and basic residues change when the redox state of the protein changes. They found that GluL212 have an anomalously broad titration curve. Their calculated free energy $\Delta G_{AB}$ of electron transfer between $Q_A^-$ and $Q_B$ was very unfavorable.

In our previous work (*13*), with different partial charge of quinone and less freedom as few conformers of residue Arg, Lys, Glu, His, Tyr *etc.*, $\Delta G_{AB}$ was calculated as –80 meV and the conformational coupling was found as in the cluster of acids (GluL212 and H173, AspL213 and L210) and SerL223. In ground state, $L212^0L213^-L210^0H173^-$ and in $Q_B^-$ state, $L212^0L213^0L210^-H173^-$, there is no charge charges in the acids cluster. Our new calculation shows that AspL210 is 100% ionized in

both ground and reduced states, because of very strongly positive polar energy from environment residues by using different L-J AB parameters.

E-W Knapp and his coworker's electrostatic calculations (*14, 27*) show that GluL212 is partially protonated (probability 0.6) in the state $Q_A^- Q_B$ and fully protonated in state $Q_A Q_B^-$, and AspL213 remains neutral in all states. This result agrees with FTIR spectra and our calculation on 1AIJ(G) structure. Our calculation also shows the protonation of GluL212 upon the reduction of $Q_B$. Based on the 1AIJ(G) structure we found that the GluL212 was 96% ionized with $Q_B$ oxidized state and fully neutral at $Q_B$ reduced state, so there is one proton uptake to GluL212 site. Meanwhile there are several Glu and His residues which partially lose protons that go to GluL212. They contribute $0.44H^+$/RC, and the other 0.52 $H^+$/RC that go to GluL212 comes from solution. They reported the $E_m(Q_A/Q_A^-)$ is around −165 mV. Their calculation did not produce reasonable $E_m(Q_B/Q_B^-)$ by trying different charge set of non-heme iron and the ligands. They focus on how the protonation of GluL212 and AspL213 could change the redox potential of $Q_A$ and $Q_B$. Their calculations showed that if the total charges on GluL212 and AspL213 are constant, the $E_m(Q_B/Q_B^-)$ at proximal site differ by 80 mV, which is little bit larger than our results (30 mV). Our calculations show that the $E_m(Q_B/Q_B^-)$ and the proton uptake vs pH are almost constant if the total charge in the acids cluster is constant.

The molecular dynamics studies have been based on the 1AIJ(G) structures. Grafton *et al.* investigated the protonation states of GluL212 and AspL213 (*21*). They propose that AspL213 is ionized not GluL212 in the $Q_B$ neutral state which agrees with our calculation on the 1M3X structure. They also found that GluL212 and AspL213 are

both neutral when $Q_B$ was reduced at the proximal site. Walden and Wheeler's MD simulation found that GluL212 can compete with $Q_B$ for the hydrogen bond with HisL190, and GluL212 was considered as a key residue to the quinone binding or migration even for the first electron transfer.

## Bibliography:


1. Deisenhofer, J., Epp, O., Miki, R., and Michel, H. (1985) Structure of the protein subunits in the photosynthetic reaction center of *Rhodopseudomonas viridis* at 3 Å resolution., *Nature 318*, 618-624.

2. Stowell, M. H. B., McPhillips, T. M., Rees, D. C., Soltis, S. M., Abresch, E., and Feher, G. (1997) Light-induced structural changes in photosynthetic reaction center: implications for mechanism of electron-proton transfer, *Science 276*, 812-816.

3. Camara-Artigas, A., Brune, D., and Allen, J. P. (2002) Interactions between lipids and bacterial reaction centers determined by protein crystallography, *Proc Natl Acad Sci USA 99*, 11055-11060.

4. Fritzsch, G., Koepke, J., Diem, R., Kuglstatter, A., and Baciou, L. (2002) Charge separation induces conformational changes in the photosynthetic reaction centre of purple bacteria, *Acta Crystallogr D Biol Crystallogr 58*, 1660-3.

5. Okamura, M. Y., Paddock, M. L., Graige, M. S., and Feher, G. (2000) Proton and electron transfer in bacterial reaction centers, *Biochim. Biophys. Acta 1458*, 148-163.

6. Paddock, M. L., Rongey, S. H., Feher, G., and Okamura, M. Y. (1989) Pathway of proton transfer in bacterial reaction centers: Replacement of glutamic acid 212 in the L subunit by glutamine inhibits quinone (secondary acceptor) turnover, *Proc. Natl. Acad. Sci. USA 86*, 6602-6606.

7. Paddock, M. L., McPherson, P. H., Feher, G., and Okamura, M. Y. (1990) Pathway of proton transfer in bacterial reaction centers: Replacement of serine-L223 by alanine inhibits electron and proton transfers associated with reduction of quinone to dihydroquinone, *Proc. Natl. Acad. Sci. 87*, 6803-6807.

8. Rongey, S. H., Paddock, M. L., Feher, G., and Okamura, M. Y. (1993) Pathway of proton transfer in bacterial reaction centers: Second-site mutation Asn-M44 --> asp restores electron ans proton transfer in reaction centers form the photosynthetically deficient Asp-L213 --> Asn mutant of *Rhodobacter sphaeroides*, *Proc. Natl. Acad. Sci. 90*, 1325-1329.

9. Paddock, M. L., Rongey, S. H., McPherson, P. H., Juth, A., Feher, G., and Okamura, M. Y. (1994) Pathway of proton transfer in bacterial reaction centers: Role of aspartate-L213 in proton transfers associated with reduction of quinone to dihydroquinone., *Biochemistry 33*, 734-745.

10. Paddock, M. L., Adelroth, P., Chang, C., Abresch, E. C., Feher, G., and Okamura, M. Y. (2001) Identification of the proton pathway in bacterial reaction centers: cooperation obetween Asp-M17 and Asp-L210 facilitates proton transfer to the secondary quinone ($Q_B$), *Biochemistry 40*, 6893-6902.

11. Nabedryk, E., Breton, J., Okamura, M. Y., and Paddock, M. L. (2001) Simultaneous replacement of Asp-L210 and Asp-M17 with Asn increases proton uptake by Glu-L212 upon first electron transfer to $Q_B$ in reaction centers from *Rhodobacter sphaeroides*, *Biochemistry 40*, 13826-13832.

12. Takahashi, E., and Wraight, C. A. (1992) Proton and electron transfer in the acceptor quinone complex of *Rhodobacter sphaeroides* reaction centers: Characterization of site-directed mutants of the two ionizable residues, Glu L212 and Asp L213, in the $Q_B$ binding site, *Biochemistry 31*, 855-866.

13. Alexov, E., and Gunner, M. (1999) Calculated protein and proton motions coupled to electron transfer: electron transfer from $Q_A^-$ to $Q_B$ in bacterial photosynthetic RCs, *Biochemistry 38*, 8253-8270.

14. Ishikita, H., Morra, G., and Knapp, E. W. (2003) Redox potential of quinones in photosynthetic reaction centers from Rhodobacter sphaeroides: dependence on protonation of Glu-L212 and Asp-L213, *Biochemistry 42*, 3882-92.

15. Hutter, M. C., Hughes, J. M., Reimers, J. R., and Hush, N. S. (1999) Modeling the bacterial photosynthetic reaction center. 2. a combined quantum mechanical/molecular mechanical study of the structure of the cofactors in the reaction centers of purple bacteria, *J. Phys. Chem 103*, 4906-4915.

16. Hughes, J. M., Hutter, M. C., Reimers, J. R., and Hush, N. S. (2001) Modeling the bacterial photosynthetic reaction center. 4 The structura,l electrochemical, and hydrogen-bonding properties of 22 mutants of *Rhodobacter sphaeroides*, *J. Am. Chem. Soc. 123*, 8550-8563.

17. Helms, V. (2002) Electronic excitations of biomolecules studied by quantum chemistry, *Curr Opin Struct Biol 12*, 169-75.

18. Hong Xu, R.-B. Z., Shu-Hua Ma, Zheng-Wang Qu, Xing-Kang Zhang & Qi-Yuan Zhang. (2002) Theoretical studies on the mechanism of primary electron transfer in the photosynthetic reaction center of Rhodobacter sphaeroides, *Photosynthesis Research 74*, 11-36.

19. Zachariae, U., and Lancaster, C. R. (2001) Proton uptake associated with the reduction of the primary quinone $Q_A$ influences the binding site of the secondary quinone $Q_B$ in *Rhodopseudomonas viridis* photosynthetic reaction centers, *Biochim Biophys Acta 1505*, 280-90.

20. Walden, S. E., and Wheeler, R. A. (2002) Protein conformational gate controlling binding site preference and migration for ubiquinone-B in the photosynthetic reactin center of *Rhodobacter sphaeroides*, *J.Phys.Chem.B 106*, 3001-3006.

21. Grafton, A. K., and Wheeler, R. A. (1999) Amino acid protonation states determine binding sites of the secondary ubiquinone and its anion in the *Rhodobacter spaeroides* photosynthetic reaction center, *J. Phys. Chem 103*, 5380-5387.

22. Schutz, C. N., and Warshel, A. (2001) What are the "dielectric constants" of proteins and how to validate electrostatic models?, *Proteins 44*, 400-417.

23. Gunner, M. R., and Alexov, E. (2000) A pragmatic approach to structure based calculation of coupled proton and electron transfer in proteins, *Biochim. Biophys. Acta 1458*, 63-87.

24. Lancaster, C. R. D., Michel, H., Honig, B., and Gunner, M. R. (1996) Calculated coupling of electron and proton transfer in the photosynthetic reaction center of *Rhodopseudomonas viridis*, *Biophys. J. 70*, 2469-2492.

25. Rabenstein, B., Ullmann, G. M., and Knapp, E.-W. (1998) Energetics of electron-transfer and protonation reactions of the quinones in the photosynthetic reaction center of *Rhodopseudonas viridis*, *Biochemistry 37*, 2488-2495.

26. Beroza, P., Fredkin, D. R., Okamura, M. Y., and Feher, R. (1995) Electrostatic calculations of amino acid titration electron transfer, $Q^-_AQ_B$---> $Q_AQ_B$-, in the reaction center, *Biophys. J. 68*, 2233-2250.

27. Rabenstein, B., Ullmann, G. M., and Knapp, E. W. (2000) Electron transfer between the quinones in the photosynthetic reaction center and its coupling to conformational changes, *Biochemistry 39*, 10487-96.

28. Alexov, E., Miksovska, J., Baciou, L., Schiffer, M., Hanson, D., Sebban, P., and Gunner, M. R. (2000) Modeling the effects of mutations on the free energy of the first electron transfer from $Q_A^-$ to $Q_B$ in photosynthetic reaction centers, *Biochemistry 39*, 5940-5952.

29. Simonson, T. (2001) Macromolecular electrostatics: continuum models and their growing pains, *Curr. Opin. Struct. Biol. 11*, 243-252.

30. Bashford, D., and Karplus, M. (1990) The $pK_a$'s of ionizable groups in proteins: Atomic detail from a continuum electrostatic model, *Biochemistry 29*, 10219-10225.

31. Yang, A.-S., Gunner, M. R., Sampogna, R., Sharp, K., and Honig, B. (1993) On the calculation of $pK_a$'s in proteins, *Proteins 15*, 252-265.

32. Beroza, P., and Case, D. (1996) Including side chain flexibility in continuum electrostatic calculations of protein titration, *J. Phys. Chem. 100*, 20156-20163.

33. You, T. J., and Bashford, D. (1995) Conformation and hydrogen ion titration of proteins: A continuum electrostatic model with conformational flexibility, *Biophys. J. 69*, 1721-1733.

34. Alexov, E. G., and Gunner, M. R. (1997) Incorporating protein conformational flexibility into the calculation of pH-dependent protein properties, *Biophys. J. 72*, 2075-2093.

35. Georgescu, R. E., Alexov, E. G., and Gunner, M. R. (2002) Combining conformational flexibility and continuum electrostatics for calculating $pK_a$'s in proteins, *Biophys J. 83*, 1731-1748.

36. Adelroth, P., Paddock, M. L., Sagle, L. B., Feher, G., and Okamura, M. Y. (2000) Identification of the proton pathway in bacterial reaction centers: Both protons associated with reduction of $Q_B$ to $Q_BH_2$ share a common entry point, *Proc. Natl. Acad. Sci. USA 97*, 13086-13091.

37. Lancaster, C. R. D. (1998) Ubiquinone reduction and protonation in photosynthetic reaction centres from *Rhodopseudomonas viridis:* X-ray strucutres and their functional implications, *Biochimica Biophysica Acta 1365*, 143-150.

38. Sridharan, S., Nicholls, A., and Honig, B. (1992) A new vertex algorithm to calculate solvent accessible surface areas., *Biophys. J. 61*, A174.

39. Bharadwaj, R., Windemuth, A., Sridharan, S., Honig, B., and Nicholls, A. (1995) The fast multipole boundary element method for molecular electrostatics: An optimal approach for large systems, *J. Comp Chem. 16*, 898-913.

40. Parson, W. W., Chu, Z.-T., and Warshel, A. (1990) Electrostatic control of charge separation in bacterial photosynthesis, *Biochim. Biophys. Acta 1017*, 251-272.

41. Sitkoff, D., Sharp, K. A., and Honig, B. (1994) Accurate calculation of hydration free energies using macroscopic solvent models, *J. Phys. Chem. 98*, 1978-1988.

42. Nicholls, A., and Honig, B. (1991) A rapid finite difference algorithm utilizing successive over-relaxation to solve the Poisson-Boltzmann equation., *J. Comp. Chem. 12*, 435-445.

43. Rocchia, W., Alexov, E., and Honig, B. (2001) Extending the applicability of the nonlinear Poisson-Boltzmann Equation: multiple dielectric constants and multivalent ions, *J. Phys. Chem. B 105*, 6507-6514.

44. Gilson, M. K., and Honig, B. (1988) Calculation of the Total Electorstatic Energy of a Macromolecular System: Solation Energies, Binding Energies, and Conformational Analysis, *Proteins 4*, 7-18.

45. Mao, J., Hauser, K., and Gunner, M. R. (2003) How cytochromes with different folds control heme redox potentials, *Biochemistry 42*, 9829-40.

46. Beroza, P., Fredkin, D. R., Okamura, M. Y., and Feher, G. (1991) Protonation of interacting residues in a protein by a Monte Carlo method: Application to Lysozyme and the photosynthetic reaction center of *Rhodobacter sphaeroides*, *Proc. Natl. Acad. Sci. USA 88*, 5804-5808.

47. Song, Y., Mao, J., and Gunner, M. R. (2003) Calculation of proton transfers in Bacteriorhodopsin bR and M intermediates, *Biochemistry 42*, 9875-88.

48. Gunsteren, W. F. v., Daura, X., and Mark, A. E. (2002) Computation of Free Energy, *Helvetica Chimica Acta 85*, 3113-3129.

49. Warncke, K., and Dutton, P. L. (1993) Influence of QA site redox cofactor structure on equilibrium binding, in situ electrochemistry, and electron-transfer performance in the photosynthetic reaction center protein, *Biochemistry 32*, 4769-79.

50. Rich, P. R. (2004) The quinone chemistry of bc complexes, *Biochim Biophys Acta 1658*, 165-71.

51. Rich, P. R., and Bendall, D. S. (1979) A mechanism for the reduction of cytochromes by quinols in solution and its relevance to biological electron transfer reactions, *FEBS Lett. 105*, 189-194.

52. Swallow, A. J. (1982) in *Function of Quinones in Energy Conserving Systems* (Trumpower, B. L., Ed.) pp 59-72, Academic Press, New York.

53. Prince, R. C., Dutton, P. L., and Bruce, J. M. (1983) Electrochemistry of ubiquinones, *Febs 160*, 273-276.

54. Wraight, C. A. (1998) in *Proceedings of the XIth International Photosynthesis Congress* (Garab, G., Ed.) pp 693-698, Kluwer, Dordrecht.

55. Morrison, L. E., Schelhorn, J. E., Cotton, T. E., Bering, C. L., and Loach, P. A. (1982) in *Function of Quinones in Energy Conserving Systems* (Trumpower, B. L., Ed.) pp 35-58, Academic Press, New York.

56. Gordillo, G. J., and Schiffrin, D. J. (2000) The electrochemistry of ubiquinone-10 in a phospholipid model membrane, *Faraday Discuss. 116*, 89-107.

57. Bishop, C. A., and Tong, L. K. J. (1965) Equilibria of Substituted Semiquinones at High pH, *J. Am. Chem. Soc. 18*, 501-505.

58. Rutherford, A. W., and Evans, M. C. W. (1980) Direct measurement of the redox potential of the primary and secondary quinone electron acceptors in *Rhodopseudomonas sphaeroides* (wild-type) by EPR spectrometry, *FEBS Lett. 110*, 257-261.

59. Gunner, M. R., Saleh, M., Cross, E., ud-Doula, A., and Wise, M. (2000) Backbone dipoles generate positive potentials in all proteins. Origins and implications of the effect., *Biophys. J. 78*, 1126-1144.

60. Lancaster, C. R. (2003) The role of electrostatics in proton-conducting membrane protein complexes, *FEBS Lett 545*, 52-60.

61. Kleinfeld, D., Okamura, M. Y., and Feher, G. (1984) Electron-transfer kinetics in photosynthetic reaction centers cooled to cryogenic temperatures in the charge separated state: Evidence for light-induced structural changes, *Biochemistry 23*, 5780-5786.

62. Xu, Q., and Gunner, M. R. (2001) Trapping conformational intermediate states in the reaction center protein from photosynthetic bacteria., *Biochemistry 40*, 3232-3241.

63. Bockris, J. O. M., and Reddy, A. K. N. (1973) *Modern Electrochemistry*, Vol. 1, Plenum, New York.

64. Ishikita, H., and Knapp, E.-W. (2004) Variation of Ser-L223 hydrogen bonding with the $Q_B$ redox state in reaction centers from *Rhodobacter sphaeroides*, *J. Am. Chem. Soc. 126*, 8059-8064.

65. Diner, B. A., Schenck, C. C., and DeVitry, C. (1984) Effect of inhibitors, redox state and isoprenoid chain length on the affinity of ubiquinone for the secondary acceptor binding site in the reaction centers of photosynthetic bacteria, *Biochim. Biophys. Acta 766*, 9-20.

66. Dutton, P. L., Leigh, J. S., and Wraight, C. A. (1973) Direct measurement of the midpoint potential of the primary electron acceptor in Rhodopsuedomonas sphaeroides in situ and in the isolated state: some relationships with pH and o-phenathroline, *FEBS Lett. 36*, 169-173.

67. Gunner, M. R., Robertson, D. E., and Dutton, P. L. (1986) Kinetic studies on the reaction center protein from *Rhodopseudomonas sphaeroides*: The temperature and free energy dependence of electron transfer between various quinones in the $Q_A$ site and the oxidized bacteriochlorophyll dimer., *J. Phys. Chem. 90*, 3783-3795.

68. Kalman, L., and Maroti, P. (1997) Conformation-activated protonation in reaction centers of the photosynthetic bacterium Rodobacter sphaeroides, *Biochemistry 36*, 15269-15276.

69. Wraight, C. A. (2004) Proton and electron transfer in the acceptor quinone complex of photosynthetic reaction centers from Rhodobacter sphaeroides, *Front Biosci 9*, 309-37.

70. Mancino, L. J., Dean, D. P., and Blankenship, R. E. (1984) Kinetics and thermodynamics of the $P870^+Q_A^-$ ‡ $P870^+Q_B^-$ reaction in isolated reaction centers from the photosynthetic bacterium *Rhodopseudomonas sphaeroides*, *Biochim. Biophys. Acta 764*, 46-54.

71. Kleinfeld, D., Okamura, M. Y., and Feher, G. (1984) Electron transfer in reaction centers of *Rhodopseudomonas sphaeroides*: I. Determination of the charge recombination pathway of $D^+Q_AQ_B^-$ and free energy and kinetic relations between $Q_A^-Q_B$ and $Q_AQ_B^-$, *Biochim. Biophys. Acta 766*, 126-140.

72. McPherson, P. H., Okamura, M. Y., and Feher, G. (1988) Light-induced proton uptake by photosynthetic reaction centers from *Rhodobacter sphaeroides* R-26. I. Protonation of the one-electron states $D^+Q_A^-$, $DQ_A^-$, $D_AQ_AQ_B^-$, and $DQ_AQ_B^-$, *Biochim. Biophys. Acta 934*, 348-368.

73. Graige, M. S., Paddock, M. L., Feher, G., and Okamura, M. Y. (1999) Observation of the protonated semiquinone intermediate in isolated reaction centers from *Rhodobacter sphaeroides*: implications for the mechanism of electron and proton transfer in proteins, *Biochemistry 38*, 11465-11473.

74. McPherson, P. H., Okamura, M. Y., and Feher, G. (1993) Light-induced proton uptake by photosynthetic reaction centers from *Rhodobacter sphaeroides* R-26.1. II. Protonation of the state $DQ_AQ_B^{2-}$, *Biochim. Biophys. Acta 1144*, 309-324.

75. McPherson, P. H., Schonfeld, M., Paddock, M. L., Okamura, M. Y., and Feher, G. (1994) Protonation and free energy changes associated with formation of $Q_BH_2$ in native and Glu-L212 --> Gln mutant reaction centers from rhodobacter sphaeroides, *Biochemistry 33*, 1181-1193.

76. Graige, M. S., Paddock, M. L., Bruce, J. M., Feher, G., and Okamura, M. Y. (1996) Mechanism of proton-coupled electron transfer for quinone ($Q_B$)

reduction in reaction centers of *Rb. Sphaeroides*, *J. Am. Chem. Soc. 118*, 9005-9016.

77. Rabenstein, B., Ullmann, G. M., and Knapp, E.-W. (1998) Calculation of protonation patterns in proteins with structural relaxation and molecular ensembles-application to the photosynthetic reaction center, *Eur. Biophys. J. 27*, 626-637.

78. Kleinfeld, D., Okamura, M. Y., and Feher, G. (1985) Electron transfer in reaction centers of *Rhodopseudomonas sphaeroides*. II. Free energy and kinetic relations between the acceptor states $Q_A^-Q_B^-$ and $Q_AQ_B^{-2}$, *Biochim. Biophys. Acta 809*, 291-310.

79. Takahashi, E., and Wraight, C. A. (1996) Potentiation of proton transfer function by electrostatic interactions in photosynthetic reaction centers from Rhodobacter sphaeroides: first results from site-directed mutation of the H subunit, *Proc. Natl. Acad. Sci. 93*, 2640-2645.

80. Paddock, M. L., Graige, M. S., Feher, G., and Okamura, M. Y. (1999) Identification of the proton pathway in bacterial reactions centers: inhibition of proton transfer by binding of $Zn^{2+}$ or $Cd^{2+}$, *Proc. Natl. Acad. Sci. USA 96*, 6183-6188.

81. Axelrod, H. L., Abresch, E. C., Paddock, M. L., Okamura, M. Y., and Feher, G. (2000) Determination of the binding sites of proton transfer inhibitor $Cd^{2+}$ and $Zn^{2+}$ in bacterial reaction centers, *Proc. Natl. Acad. Sci. USA 97*, 1542-1547.

82. Paddock, M. L., Adelroth, P., Feher, G., Okamura, M. Y., and Beatty, J. T. (2002) Determination of proton transfer rates by chemical rescue: application to bacterial reaction centers, *Biochemistry 41*, 14716-25.

83. Maroti, P., and Wraight, C. A. (1988) Flash-induced $H^+$ binding by bacterial photosynthetic reaction centers: Influences of the redox states of the acceptor quinones and primary donor, *Biochim. Biophys. Acta 934*, 329-347.

84. Sebban, P., Maroti, P., and Hanson, D. K. (1995) Electron and proton transfer to the quinones in bacterial photosyntheic reaction centers: Insight from combined approaches of molecular genetics and biophysics, *Biochimie 77*, 677-694.

85. Gunner, M. R., Nicholls, A., and Honig, B. (1996) Electrostatic potentials in *Rhodopseudomonas viridis* reaction center: Implications for the driving force and directionality of electron transfer., *J. Phys. Chem. 100*, 4277-4291.

86. Ermler, U., Fritzsch, G., Buchanan, S. K., and Michel, H. (1994) Structure of the photosynthetic reaction centre from *Rhodobacter sphaeroides* at 2.65 Å resolution: cofactors and protein-cofactor interactions, *Structure 2*, 925-936.

87. Lancaster, R., and Michel, H. (1997) The coupling of light-induced electron transfer and proton uptake as derived from crystal structures of reaction centers from *Rhodopseudomonas viridis* modified at the binding site of the secondary quinone, QB, *Structure 5*, 1339-1359.

88. Fyfe, P. K., and Jones, M. R. (2000) Re-emerging structures: continuing crystallography of the bacterial reaction centre, *Biochim. Biophys. Acta 1459*, 413-421.

89. Paddock, M. L., Feher, G., and Okamura, M. Y. (2003) Proton transfer pathways and mechanism in bacterial reaction centers, *FEBS Lett 555*, 45-50.

90. Kirmaier, C., Holten, D., and Parson, W. W. (1985) Temperature and detection-wavelenth dependence of the picosecond electron transfer kinetics measured in *Rhodopseudomonas sphaeroides* reaction centers. Resolution of new spectral and kinetic compontents in the primary charge separation process, *Biochim. Biophys. Acta 810*, 33-48.

91. Graige, M. S., Feher, G., and Okamura, M. Y. (1998) Conformational gating of the electron transfer reaction $Q_A^- Q_B \ddagger Q_A Q_B^-$ in bacterial reaction centers of *Rhodobacter sphaeroides* determined by a driving force assay, *Proc. Natl. Acad. Sci. USA 95*, 11679-11684.

92. Li, J., Gilroy, D., Tiede, D. M., and Gunner, M. R. (1998) Kinetic phases in the electron transfer from $P^+Q_A^-Q_B$ to $P^+Q_AQ_B^-$ and the associated processes in *Rhodobacter sphaeroides* R-26 reaction centers., *Biochemistry 37*, 2818-2829.

93. McPherson, P. H., Okamura, M. Y., and Feher, G. (1990) Electron transfer from the reaction center of *Rb. sphaeroides* to the quinone pool: doubly reduced $Q_B$ leaves the reaction center, *Biochim. Biophys. Acta 1016*, 289-292.

94. Breton, J., Boullais, C., Mioskowski, C., Sebban, P., Bacious, L., and Nabedryk, E. (2002) Vibrational spectroscopy favors a unique $Q_B$ binding site at the proximal position in wild-type reaction centers and in the Pro-L209 ‡ Tyr mutant from *Rhodobacter sphaeroides*, *Biochemistry 41*, 12921-12927.

95. Xu, Q., Baciou, L., Sebban, P., and Gunner, M. R. (2002) Exploring the energy landscape for $Q_A^-$ to $Q_B$ electron transfer in bacterial photosynthetic reaction centers: Effect of substrate position and tail length on the conformational gating step., *Biochemistry 41*, 10021-10025.

96. Pokkuluri, P. R., Laible, P. D., Crawford, A. E., Mayfield, J. F., Yousef, M. A., Ginell, S. L., Hanson, D. K., and Schiffer, M. (2004) Temperature and cryoprotectant influence secondary quinone binding position in bacterial reaction centers, *FEBS Let. 570*, 171-174.

97. Remy, A., and Gerwert, K. (2003) Coupling of light-induced electron transfer to proton uptake in photosynthesis, *Nature Struc. Biology 10*, 637-644.

98. Warncke, K., and Dutton, P. L. (1993) Experimental resolution of the free energies of aqueous solvation contributions to ligand-protein binding: quinone-$Q_A$ site interactions in the photosynthetic reaction center protein, *Proc. Natl. Acad. Sci. USA 90*, 2920-2924.

99. McComb, J. C., Stein, R. R., and Wraight, C. A. (1990) Investigations on the influence of headgroup substitution and isoprene side-chain length in the function of primary and secondary quinones of bacterial reaction centers, *Biochim. Biophys. Acta 1015*, 156-171.

100. Graige, M. S., Feher, G., and Okamura, M. Y. (1998) Conformational gating of the electron transfer reaction $Q_A^-Q_B$ -> $Q_AQ_B^-$ in bacterial reaction centers of *Rhodobacter sphaeroides* determined by a driving force assay, *Proc. Natl. Acad. Sci. USA 95*, 11679-11684.

101. Li, J., Takahashi, E., and Gunner, M. R. (2000) $-\Delta G°_{AB}$ and pH dependence on the electron transfer from $P^+Q_A^-Q_B$ to $P^+Q_AQ_B^-$ in *Rhodobacter sphaeroides* reaction centers, *Biochemistry 39*, 7445-7454.

102. Kuglstatter, A., Ermler, U., Michel, H., Baciou, L., and Fritzsch, G. (2001) X-ray structure analyses of photosynthetic reaction center variants from *Rhodobacter sphaeroides*: structural changes induced by point mutations at position L209 modulate electron and proton transfer, *Biochemistry 40*, 4253-60.

103. Baxter, R. H. G., Ponomarenko, N., Srajer, V., Pahl, R., Moffat, K., and Norris, J. R. (2004) Time-resolved crystallographic studies of light-induced structural changes in the photosynthetic reaction centers, *Proc. Natl. Acad. Sci. USA 101*, 5982-5987.

104. Taly, A., Sebban, P., Smith, J. C., and Ullmann, G. M. (2003) The position of QB in the photosynthetic reaction center depends on pH: a theoretical analysis of the proton uptake upon QB reduction, *Biophys J 84*, 2090-8.

105. Sebban, P., Maroti, P., Schiffer, M., and Hanson, D. K. (1995) Electrostatic dominoes: Long distance propagation of mutational effects in photosynthetic reaction centers of *Rhodobacter capsulatus*, *Biochemistry 34*, 8390-8397.

106. Nabedryk, E., Breton, J., Joshi, H. M., and Hanson, D. K. (2000) Fourier transform infrared evidence of proton uptake by glutamate L212 upon reduction of the secondary quinone($Q_B$) in the photosynthetic reaction center from *Rhodobacter capsulatus*, *Biochemistry 39*, 14654-14663.

107. Mezzetti, A., Nabedryk, E., Breton, J., Okamura, M. Y., Paddock, M. L., Giacometti, G., and Leibl, W. (2002) Rapid-scan Fourier transform infrared spectroscopy shows coupling of GLu-L212 protonation and electron transfer to Q(B) in Rhodobacter sphaeroides reaction centers, *Biochim Biophys Acta 1553*, 320-30.

108. Lavergne, J., Matthews, C., and Ginet, N. (1999) Electron and proton transfer on the acceptor side of the reaction center in chromatophores of *Rhodobacter capsulatus:* Evidence for direct protonation of the semiquinone state of $Q_B$, *Biochemistry 38*, 4542-4552.

109. Rinyu, L., Martin, E. W., Takahashi, E., Maroti, P., and Wraight, C. A. (2004) Modulation of the free energy of the primary quinone acceptor $Q_A$ in reaction centers from *Rhodobacter sphaeroides*: contributions from the protein and protein-lipid(cardiolipin) interactions, *Biochim Biophys Acta 1655*, 93-101.

110. Ginet, N., and Lavergne, J. (2000) Interactions between the donor and acceptor sides in bacterial reaction centers, *Biochemistry 39*, 16252-62.

111. Kleinfeld, D., Abresch, E. C., Okamura, M. Y., and Feher, G. (1984) Damping of oscillations in the semiquinone absorption in reaction centers after successive flashes: determination of the equilibrium between Qa-Qb and QaQb-, *Biochim. Biophys. Acta 765*, 406-409.

112. Gunner, M. R., and Zhu, Z. (2004) Protons forge new paths, *Structure (Camb) 12*, 518-9.

113. Xu, Q., Axelrod, H. L., Abresch, E. C., Paddock, M. L., Okamura, M. Y., and Feher, G. (2004) X-ray structure determination of three mutants of the bacterial photosynthetic reaction centers from Rhodobacter sphaeroides: altered proton transfer pathways, *Structure (Camb) 12*, 703-15.

114. Kannt, A., Lancaster, C. R. D., and Michel, H. (1998) The coupling of electron transfer and proton translocation: electrostatic calculations on *Paracoccus denitrificans* cytochrome c oxidase, *Biophys J 74*, 708-21.

115. Sampogna, R. V., and Honig, B. (1994) Environmental effects on the protonation states of active site residues in bacteriorhodopsin, *Biophys J 66*, 1341-52.

116. Sampogna, R. V., and Honig, B. (1996) Electrostatic Coupling between Retinal Isomerization and the Ionization State of Glu-204: A General Mechanism for Proton Release in bacteriorhodopsin, *Biophys. J. 71*, 1165-1171.

117. Bashford, D., and Gerwert, K. (1992) Electrostatic calculations of the $pK_a$ values of ionizable groups in bacteriorhodopsin, *J. Mol. Biol. 224*, 473-486.

118. Antosiewicz, J., McCammon, J. A., and Gilson, M. K. (1994) Prediction of pH-dependent properties in proteins, *J. Mol. Biol. 238*, 415-436.

119. Brzezinski, P., Paddock, M. L., Okamura, M. Y., and Fehr, G. (1997) Light-induced electrogenic events associated with proton uptake upon forming QB- in bacterial wild-type and mutant reaction centers, *Biochim Biophys Acta 1321*, 149-156.

120. Paddock, M. L., Feher, G., and Okamura, M. Y. (1997) Proton and electron transfer to the secondary quinone ($Q_B$) in bacterial centers: the effect of changing the electrostatics in the vicinity of $Q_B$ by interchanging Asp and Glu at the L212 and L213 sites, *Biochemistry 36*, 14238-14249.

121. Hienerwadel, R., Thibodeau, D., Lenz, F., Nabedryk, E., Breton, J., Kreutz, W., and Mantele, W. (1992) Time-resolved infrared spectroscopy of electron transfer in bacterial photosynthetic reaction centers: Dynamics of binding and interaction upon $Q_A$ and $Q_B$ Reduction, *Biochemistry 31*, 5799-5808.

122. Hienerwadel, R., Grzybek, S., Fogel, C., Kreutz, W., Okamura, M. Y., Paddock, M. L., and Breton, J. (1995) Protonation of Glu L212 following $Q_B$-formation in the photosynthetic reaction center of *Rhodobacter sphaeroides*: Evidence from time-resolved infrared spectroscopy, *Biochemistry 34*, 2832-2843.

123. Nabedryk, E., Brenton, J., Hienderwadel, R., Fogel, C., Mantele, W., Paddock, M. L., and Okamura, M. Y. (1995) Fourier transform infrared difference spectroscopy of secondary quinone acceptor photoreduction in proton transfer mutants of *Rhodobacter spaeroides*, *Biochemistry 34*, 14722-14732.

124. Nabedryk, E., Breton, J., Okamura, M. Y., and Paddock, M. L. (1998) Proton uptake by carboxylic acid groups upon photoreduction of the secondary quinone ($Q_B$) in bacterial reaction centers from *Rhodobacter sphaeroides*: FTIR studies on the effects of replacing GLU H173, *Biochemistry 37*, 14457-14462.